1 MBR simulation of miniplug energy deposition

This study was done using the MBR output files for "hard-core", double-diffractive (DD), and single-diffractive events used in the inclusive DD cross section measurement. The number of each type of interaction was based on the measured cross sections. Events were required to have particles in the east and west CLC ($3.75 < |\eta| < 4.75$) in order to compare with minimum-bias data. The study involved only single interactions.

MBR only generates pions (and leading nucleons). For π^0s, the energy in the miniplug was taken to be the energy of the π^0. For charged pions, based on the fact that the miniplug is a little more than one interaction length, 70% of the time the energy was taken from a gaussian with a mean μ of 1/3 of the $\pi^{\pm}$ energy and $\sigma = \mu/2$. The other 30% of the time, the energy was taken from a landau distribution with peak $E_{mip} = 0.5$ GeV and width 25%(E_{mip}). That means the energy deposited in the miniplug is on average about 40-50% of a true particle energy.

Fig. 1 shows MiniPlug tower geometry in the plane perpendicular to the beam. The detector has 84 towers each and the towers make four layers (12, 18, 24 and 30 towers per layer). Due to the structure of the detector, each tower has slightly different coverage in both η and ϕ, but we approximate the towers in each layer to have the same coverage in the simulation. The η coverage in each of four layers is shown in the figure.

Fig. 2 shows an double exponential fit (given below) of the energy per tower in each of the four tower layers at a given instantaneous luminosity;

$$F_{fit}(E) = p1 \cdot exp(p2 \cdot E) + p3 \cdot exp(p4 \cdot E) \qquad (p4 < p2 < 0), \tag{1}$$

where E is the energy in GeV, $p4$ ($p2$) is the slope of the first (second) exponential fit. If in a given event there are no particles going into a tower, no entry is made in the histogram for that tower. The energy per tower was examined at different luminosity intervals between 5E30 and 35E30 and the slopes didn't show any appreciable change with instantaneous luminosity. We use the $p4$ values in the figure to calibrate the MiniPlug energy in data (Table 1).

Table 1: Simulation slopes of the energy per tower in each of four η-layers of MiniPlug.

Layer#	0	1	2	3
η range	$4.55 < \|\eta\| < 5.20$	$4.20 < \|\eta\| < 4.55$	$3.95 < \|\eta\| < 4.20$	$3.70 < \|\eta\| < 3.95$
Slope	-0.099	-0.156	-0.171	-0.199

2 MiniPlug Calibration with the Simulation

Two approaches were originally used to calibrate MiniPlug energy by taking into account effects of multiple interactions in real data. Both approaches are based on looking at the slope of measured ADC count distributions in minimum bias (CLC east-west coincidence) data. One is to look at the distributions in different instantaneous luminosity intervals and derive the "luminosity dependent" calibrations. The other is to look at the distributions for events with 0 or 1 reconstructed vertex to obtain "luminosity independent" calibrations (to first order) then apply additional corrections based on the number of vertices in case more than one vertices are found in the event. For the latter we assumed that the MiniPlug energy would not depend on the instantaneous luminosity in single vertex events. However, further studies showed that the MiniPlug PMT gain shows luminosity dependence even in single interaction events. From the observation we decided to focus on the "luminosity dependent" calibrations which would take into account the change of PMT gains.

General procedure of the calibration is the following. We first obtain the slopes of data ADC distributions for each tower in different luminosity ranges without any vertex cuts. The slopes of data (s_{data}) are then scaled by the energy slopes of the towers obtained from MBR simulation (s_{sim}), discussed in the previous section. The ratio of the data-ADC slope to the simulation-energy slope is used to obtain tower energy from raw ADC count at a given instantaneous luminosity of an event;

$$E_{tower} = \left.\frac{s_{data}}{s_{sim}}\right|_{L} \times ADC_{tower}. \tag{2}$$

We have to, however, note that the slopes in the simulation (s_{sim} in Table 1) are obtained from deposited energy of particles that directly hit a given tower. Therefore, we used two steps to obtain the slope ratio in Eq. 2. In the first step we use all MiniPlug towers in each event of minimum bias data and make the ratios using s_{sim} in Table 1. Using these ratios as in Eq. 2 we obtain a preliminary calibrated energy for each tower. We call this step "Pass 1" calibration. The Pass 1 calibration serves to equalize the tower-by-tower variation of gain within a same η-layer and normalize tower energies of data to have the same η dependence of energy as that in the simulation. We then use the Pass 1 calibrated energy of towers to look for "seed" towers (defined as a highest E_T tower in a group of towers which consists of a tower and its neighboring towers in each MiniPlug detector) in each event. From the ADC count slopes of the seed towers we calculate the data to simulation ratio of the slope again. Using these slope ratios in Eq. 2 is called "Pass 2" calibration hereafter. In this procedure we assume that the seed tower is a tower which a particle hits.

Electromagnetic particles (such as π^0) make shower in the MiniPlug and all the particle energy may not be deposited in a seed tower due to towerless structure of MiniPlug. The leakage of energy from a seed tower due to this "energy sharing" effect indeed exists in real data (as described later). This effect is not taken into account in the simulation. Therefore, we need to correct the data for this effect to obtain a particle energy deposited

Table 2: Ranges of runs with four different high voltage settings of MiniPlug. The first and last long run ranges are further split into three and four subsamples, respectively, in the analysis. The last column gives links to the text file of each HV setting.

Run Range	Date	#MB Events	Luminosity	MP-HV
151648-153091	9/17/02-10/21/02	798K	12.9 pb^{-1}	(1)
153266-154861	10/24/02-12/03/02	1,385K	24.0 pb^{-1}	(1)
155107-160065	12/05/02- 3/11/03	1,165K	20.3 pb^{-1}	(1)
160090-160442	3/11/03- 3/21/03	321K	6.4 pb^{-1}	(2)
160533-162521	3/21/03- 5/ 6/03	1,466K	29.2 pb^{-1}	(3)
162631-163960	5/ 7/03- 6/ 2/03	710K	16.3 pb^{-1}	(4)
164107-165523	6/ 3/03- 7/ 2/03	1,056K	18.9 pb^{-1}	(4)
165836-167061	7/ 7/03- 8/ 5/03	1,220K	25.5 pb^{-1}	(4)
167137-168889	8/ 6/03- 9/ 6/03	983K	22.1 pb^{-1}	(4)

in the detector that is to be compared with the simulation. Questions regarding the energy sharing (how much particle energy leaks out of a seed tower? whether it depends on the energy or not? if so, how?) will be addressed in Section 2.3.

2.1 "Pass 1" Luminosity Dependent Calibration

We used all available CLC minimum bias data (runs 151648-168889) collected from Summer 2002 until Fall 2003 shutdown. The run 151683 is the first good run of physics data for the forward detectors. First, good runs for calorimetry, COT, CLC and all 3 level triggers were selected. MiniPlug and BSC bad runs were then removed. We have lowered three times the high voltages of the MiniPlug since run 151683, and the data were therefore grouped into four subsamples, each of which has a fixed high voltage setting. In addition, two long periods of those four subsamples, i.e, runs 151648-160065 and runs 162631-168889, are further grouped into three and four small samples respectively, each of which has about 20 pb^{-1} of data, to account for possible gain degradation of MiniPlug PMTs. The list of nine run intervals is given in Table 2. After removing the bad runs, the data were split into different luminosity intervals with 5E30 pitch, then the raw ADC count distributions of all towers in each interval were fit with double exponential function;

$$F_{fit}(x) = p0 \cdot exp(-x/p1) + p2 \cdot exp(-x/p3) \qquad (p0 > p2). \tag{3}$$

Using double exponential function is motivated by the shape of ADC distribution with different slopes, as shown in Figs 3 and 4. These figures show the ADC count distributions of the West MiniPlug tower #0 and #12, respectively, for six luminosity intervals in the sample of runs 151648-153091. The data in the luminosity greater than 35E30 was a few so not plotted. The slope parameter -1/$p1$ in the first exponential function is plotted as a function of luminosity in the bottom-left plot. It turned out that the slope (negative

value) shows a smooth linear relationship with instantaneous luminosity for all towers. Fitting the slope versus instantaneous luminosity with a linear function would therefore provide the slope at a given instantaneous luminosity in which an event is recorded.

The fit linear functions for the two West MiniPlug towers (#0 and #12) are shown in the left plots of Fig. 5 for all the nine subsamples. They are basically well similar to each other within the fit uncertainties for the tower #0, while the tower #12 shows the ADC slope became steeper (by 0.0002) independently of luminosity, that is due to lowering the HV from 620V to 605V for the PMT#12 which the tower belongs to. Time dependence of the slope is also an interesting piece of information as it should tell the gain stability over time. Right plots of Fig. 5 show the slope parameters of those two towers at a fixed instantaneous luminosity (2E31) against integrated luminosity accumulated over all samples (about 180 pb^{-1} in total). No appreciable change of slope is seen for both towers except the drop of 0.0002 at about 65 pb^{-1} due to the change of PMT HV for tower #12. There is an indication of decreasing slope by about 15% over the first 60 pb^{-1} period for tower #12. Change of slope cannot be seen after the HV was lowered. This decrease of the slope is essentially consistent with what we see in LED calibration data for the MiniPlug (described later).

The data slopes (which are luminosity dependent) divided by simulation slopes (in Table 1) provide Pass 1 ADC to GeV conversion constants. Processing all minimum bias data with the conversion constants as in Eq. 2, we obtain Pass 1 calibrated energy for towers. Figs. 6 and 7 show the mean values of raw ADC counts (open points) and Pass 1 calibrated energy (filled points) for four different layers in West and East MiniPlugs, respectively, in the first run interval (runs 151648-153091). The horizontal axis in each plot covers the range $0 < \phi < 2\pi$ in the same η-layer. MiniPlug tower responses become flat (within $\pm 20\%$) in ϕ after calibration, that means tower-by-tower variation is rather well corrected with this calibration.

Figs. 8 (Fig. 9) shows the mean E_T of West (East) MiniPlug towers after the calibration at an instantaneous luminosity of 1.0-1.5E31 for all nine run intervals. The plots are shown again for four different η-layers. In general all nine distributions have similar mean E_T in each η-layer, and this is simply because the nine subsamples of data were normalized to the same simulation.

2.2 "Pass 2" Luminosity Dependent Calibration

Given that the tower energy in minimum bias events is well equalized by Pass 1 calibration, we proceed to a next (Pass 2) calibration procedure. For the same minimum bias data of nine run intervals, we performed fits to the ADC count distributions of seed towers with $E_T > 200$ MeV obtained using Pass 1 calibration. We find that now many seed towers (especially in inner η-layers) are well fit by a single exponential function instead of double exponential. Also, it turned out that the seed towers in inner η-layers show the presence of a peak in ADC counts but those in outer layers don't show, as shown in Figs 10 and 11. This could be presumably due to that selecting a highest E_T tower in several adjacent towers is almost equivalent to requiring the tower to have energy above a level of some

background (multiple interactions, beam remnant etc.) in a given η-layer. From these observations we use a single exponential fit for inner three layers and fit it to ADC data after the peak. It appears the seed towers in the most outer layer are still well fit by a double exponential, so we use it in the fit.

Figs 10 and 11 show the ADC count distributions of the West MiniPlug "seed" tower #0 and #12, respectively, for six luminosity intervals in the sample of runs 151648-153091. The slope parameter -1/$p1$ of the first exponential fit is plotted as a function of luminosity in the bottom-left plot. The slope for seed towers changes linearly with instantaneous luminosity as well as the case of all towers for Pass 1 calibration, but overall luminosity dependence of the slope is less significant.

Linear fits to the slope parameter versus instantaneous luminosity of the West MiniPlug seed tower #0 and #12 are shown in Fig. 12 (left) for all the nine subsamples. Comparing with corresponding plots for the towers in all events (Fig. 5), the overall slope values are more than 50% smaller (in absolute value) when the towers are required to be seed. Shown in the right plots of Fig. 12 are the slope as a function of integrated luminosity for the seed towers. No significant change of slope at a fixed HV is seen for both seed towers.

The data slopes (which are luminosity dependent) of seed towers divided by simulation slopes (Table 1) provide Pass 2 ADC to GeV conversion constants. The constants obtained at an instantaneous luminosity of 2E31 (which is more or less average luminosity of all samples) are plotted in Figs 13-21 for all 84+84 towers in each run interval of Table 2 (actually shown is the energy in GeV per 1000 ADC counts). We see a clear structure in the constants as a function of tower number due to difference in PMT gains. The mean value of the energy per 1000 ADC counts has been changed from about 0.7 GeV (Fig. 13) to 1.2 GeV (Fig. 21) mainly due to lowering the gain of some PMTs. At a fixed HV (Figs. 13-15 or 18-21) the mean energy is well stable. Also the distributions are more broader in later runs for the same reason.

2.3 Energy Sharing in a MiniPlug Detector

Due to towerless geometry of the MiniPlug, the shower energy developed in a MiniPlug detector could spread from a tower hit by a particle to neighboring towers. We use the highest E_T tower in a group of towers consisting of a tower and its neighbors (i.e, Pass 2 calibration) in the tower energy calibration. The leakage of energy from the seed tower must be quantified and it will have to be corrected in data because the energy sharing effect is not considered in the MBR simulation.

We first selected events with only one seed tower with E_T above some thresholds in an entire detector from minimum bias data, and looked at the energy of all towers. Here we used the Pass 2 calibration constants to obtain the tower energy. Fig. 22 shows the average energy of MiniPlug towers along the ϕ in each of four η-layers of the detector. If only one seed tower with $E_T > 400$ MeV is found in a detector, the energy of towers in a layer which the seed tower belongs to is plotted on the ϕ value relative to the seed tower which is always positioned at $\phi = 0$. The shower energy originated from particle hitting

the seed tower may be obtained by subtracting a flat energy component (that we get from towers at $|\phi| > 90°$) from the peak energy. A magnitude of the flat energy depends on the E_T cut of the seed tower and also on the η-layers. Figs. 23 and 24 show the cases of seed tower with $E_T > 200$ MeV and $E_T > 100$ MeV, respectively. It appears the flat energy scales very well with the choice of seed tower E_T cuts. Subtracting the magnitude of flat energy from all towers and dividing the energy of towers by the energy of seed tower, we could obtain the fractional energy of towers adjacent to the seed in ϕ, as shown in Fig. 25 for the seed tower $E_T > 400$ MeV. About 30% (10%) of seed tower's energy goes to the neighbors (next to neighbors) each in ϕ, and this looks similar to all four layers. This behavior is examined in different instantaneous luminosity ranges as shown in the plots. The energy levels of seed tower and flat component, and also the energy sharing in ϕ look all stable (except the last luminosity bin with poor statistics). Not shown but results for different seed tower E_T cuts ($E_T > 200$ MeV and 100 MeV) also look very similar.

Attempts to obtain the energy sharing in two dimensional detector plane perpendicular to the beam were done in a similar way. Shown in Fig. 26 are the average energy of West MiniPlug towers displayed in X-Y plane for events with only one seed tower at a position which is denoted in each plot. Given that the tower response is well equalized in a given η-layer, the plot is made first by identifying the location of the seed tower in each 60-degree section (see Fig. 1) and then rotating all towers in a detector such that the seed tower is always positioned in the first 60-degree section (tower #0-#13). Therefore, fourteen plots corresponding to fourteen towers in the first section are available. Subtracting the constant energies obtained from Fig. 22 on a layer-by-layer basis and dividing the tower energies by the energy of seed, we can obtain the two dimensional fractional energy of towers relative to the seed (Fig. 27). The plots provide us information about the size of a particle shower in a MiniPlug detector. It is seen that almost all energy of the shower is deposited in a seed plus adjacent towers in three concentric layers surrounding the seed. One should however note that some amount of particle energy is lost due to limited detector coverage. If an EM particle were hitting one of the towers #2-#8, large fraction of its shower would be covered by the detector, but if it hits one of #9-#13, large fraction of the shower energy will not be deposited in the detector on the contrary. The loss of particle energy may be estimated by averaging measured tower energies in a given concentric layer surrounding the seed and assuming the average energy in "virtual" towers that are actually not instrumented.

Fig. 28 shows the average "uncorrected" energy deposited in a seed plus adjacent towers in zero, one, two and three concentric layers for West MiniPlug. Uncorrected energy indicates it is the energy measured by the detector and is not corrected for energy loss described above. The energy in the plot is normalized to the 4th bin (seed plus three concentric towers). The same distributions for East MiniPlug are shown in Fig. 29. It appears that about 20-30% of a particle shower energy is left in a seed, and the rest 30-40%, 20% and 10-15% of energy are deposited in towers in the first, second and third layers, respectively, surrounding the seed. These relative uncorrected energy fractions look indeed depending on which tower the particle hits. When the energy loss is taken into account ("corrected" energy in the plots), the relative energy fractions show a better

Table 3: Fractional energy of a seed tower to the sum of the seed and towers in three concentric layers surrounding the seed for each of fourteen seed tower positions (see Fig. 1). Energy loss of limited detector coverage is corrected as described in the text.

Tower#	Fraction	Tower#	Fraction
0	0.267	7	0.228
1	0.255	8	0.240
2	0.214	9	0.202
3	0.218	10	0.250
4	0.220	11	0.247
5	0.231	12	0.249
6	0.234	13	0.250

agreement for all towers; 20-25% in the seed, 40%, 20% and 10-15% in the first, second and third layers surrounding the seed. Agreement between West and East MiniPlugs looks excellent.

Fig. 30 (Fig. 31) shows the average corrected energy fractions for West (East) MiniPlug with different E_T thresholds for seed towers. It appears the energy fractions are really independent of energy deposited in the seed tower. From this we obtain a correction factor to correct back the seed tower energy to a particle energy deposited in a detector according to the tower position (#0-#13), as given in Table 3. The data slope s_{data} of "particle energy" registered in a detector can be therefore obtained by multiplying the s_{data} which we got using seed towers in Sec. 2.2 by these correction factors because the correction is independent of the seed tower energy. Accordingly the calibration constants obtained in Sec. 2.2 will then have to be multiplied by the same factors. For example, 0.7 GeV energy per 1000 ADC counts of a given tower (Fig. 13) may now correspond to about 0.18 GeV.

3 Di-Jet Balancing Technique for MiniPlug Calibration

It is well known that di-jet balancing (equal transverse energy of the two jets in pure dijet sample) can be used to calibrate the energy scale of the calorimeters. This technique was adopted in MiniPlug energy calibration as a cross-check of what we obtained from the calibration based on the simulation.

We used a sample of events collected with a single calorimeter tower $E_T > 5$ GeV in runs 151683-155107, corresponding to about 34 pb^{-1} of data. The same bad runs were removed from the sample. To reduce multiple interaction background in the sample, we used only data collected at the instantaneous luminosity below 2E31, then applied the single vertex cut (zero or one reconstructed vertex) to the remaining sample. If the

vertex is found, it was required to be within ±60 cm in Z. For jets we applied the full energy corrections (level 7) with jet energy correction of version 4. Then we created two subsamples from them: 1) a main sample which consists of events with only one jet in the central calorimeter ("one-jet" sample), and 2) a control sample that contains events with two good dijets ("di-jet" sample). For 1) we required the leading jet to be in the range $0.1 < |\eta_{det}| < 0.7$ and have $E_T > 5$ GeV (all leading jets passed the E_T cut, though). We also demanded "no jets" in the plug. For 2) we required the two leading jets to be in the range $|\eta_{det}| < 2.5$ and good back-to-back ($\Delta\phi_{jj} > 2.7$). In addition, the 2nd jet's corrected E_T was required to be greater than 80% of the leading jet E_T, and the 3rd jet (if exists) to have E_T less than 5 GeV.

3.1 Tower Level Distributions

Fig. 32 shows the scalar-sum of E_T for the MiniPlug calorimeter towers with $E_T > 20$ MeV (top), azimuthal angle ϕ of the vector-sum of the towers (middle) and the difference of ϕ between the MiniPlug tower vector-sum and the leading jet in the central calorimeter (bottom). The Pass 2 calibration constants corrected for the energy loss factors in Table 3 were used to obtain MiniPlug tower energy. And the energy was further corrected for the Z position of the primary vertex. The scaler E_T sum looks similar but it also appears one-jet sample contains more events with high E_T in MiniPlug than di-jet sample. The $\Delta\phi$ plots show the energy deposited in the MiniPlug towers tends to be more back-to-back to the leading jet in one-jet sample than in di-jet sample, which might indicate the presence of a counterpart to the leading jet in MiniPlug in one-jet sample.

3.2 Definition of MiniPlug Jet

We need to define "miniplug jet" which may be a counterpart of the leading jet in the central calorimeter for di-jet balancing. In this study a miniplug jet is defined as a vector pointing to a seed tower (obtained as done in Sec. 2), whose energy is taken to be the energy of the seed tower plus towers in three concentric layers surrounding the seed (corrected for energy loss described in Sec. 2.3). The MiniPlug tower energy is obtained in the same way as above. The minimum E_T of seed tower is chosen to be 400 MeV. To obtain clean miniplug jet sample the data with at most one miniplug jet in either detector is selected.

3.3 MiniPlug Jet Distributions

Fig 33 shows E_T, energy, ϕ and $\Delta\phi$ of the miniplug jets in each detector for one-jet (solid) and di-jet (dashed) samples. In examining these plots it turned out that the miniplug jets show very low E_T around $2 \sim 3$ GeV when the seed tower of the jet is in either of two inner tower layers. The plots of Fig. 33 are for miniplug jets with a seed tower in the most outer layer. They are very similar to each other in two samples except the $\Delta\phi$ plot showing more back-to-back behavior in one-jet sample. E_T correlations between the leading jet

in the central calorimeter and the miniplug jet are shown in Fig 34. Many miniplug jets populate in the E_T range below 4 GeV and they don't show any clear correlation with respect to the leading jet in both one-jet (middle plot) and di-jet (bottom plot) samples. These "jets" may not be real jets but some particles which are not associated with the jet system, such as beam remnant or soft multiple interactions. However, there are some higher E_T jets in the miniplug (above 4 GeV). The $\Delta\phi$ between the miniplug jets with $E_T > 4$ GeV and the central leading jet is shown in the top of Fig 34. One-jet sample clearly shows back-to-back behavior of the miniplug jets, while it is flat in di-jet sample.

The back-to-back peak (let's say $\Delta\phi > 2.7$) of miniplug jets in one-jet sample might be likely regarded as a counterpart of the leading jet, so a variable β, defined as the E_T of the miniplug jet divided by the leading jet E_T, would tell us the energy scale of miniplug jet. Fig 35 shows the β for both detectors in one-jet sample. The β distributions have a peak at $\beta = 0.4$ with $\sigma = 0.1$, which indicates that about 40% of real jet energy is measured in the MiniPlug. This is consistent with our assumption used in the simulation.

4 Comment on PMT Gain

Fig 36 (Fig. 37) show the West (East) MiniPlug PMT response to the LED as a function of time (run number) for four month periods between Aug. 5th, 2002 and Dec. 18th, 2002. The plots show that the LED responses continuously dropped for all PMTs by $5 \sim 15\%$ for that period. This is actually consistent with what we observed in Fig. 5 showing the ADC count slope of the West MiniPlug tower #0 and #12 versus integrated luminosity. The behavior of decreasing LED response looks more pronounced in outer PMTs than in inner ones, and it is seen in Fig. 5 showing no visible change of slope for tower #0 that is in an inner PMT but recognizable slope decrease for tower #12 which belongs to an outer PMT, for the first 65 pb^{-1} period.

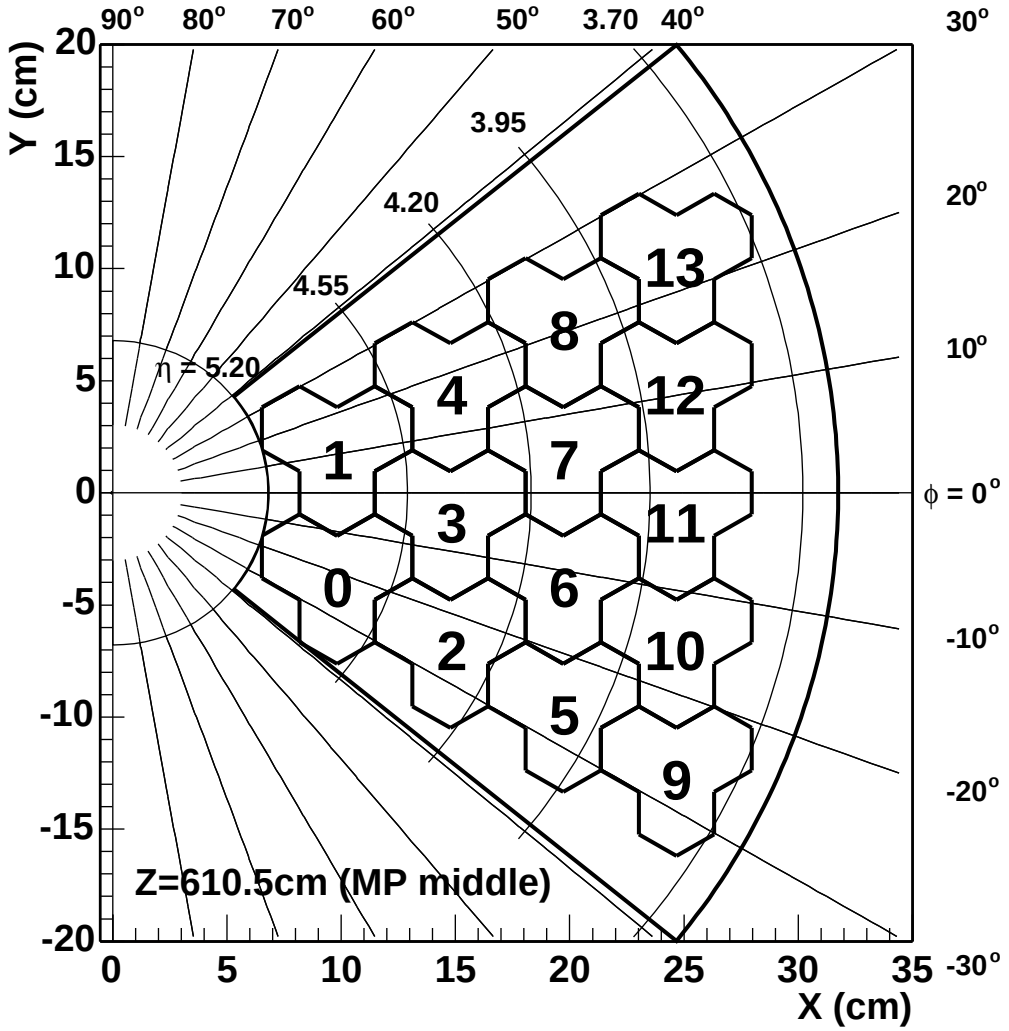

Figure 1: Cross section of a first 60° section in ϕ of MiniPlug detector in the plane perpendicular to the beam at $Z = 610.5$ cm which is the middle of the MiniPlug in Z. A 60° section consists of fourteen towers and each tower is comprised of three hexagons. The center of the beam pipe is at (0,0). η values in the plot defines the η coverage of each of four tower layers.

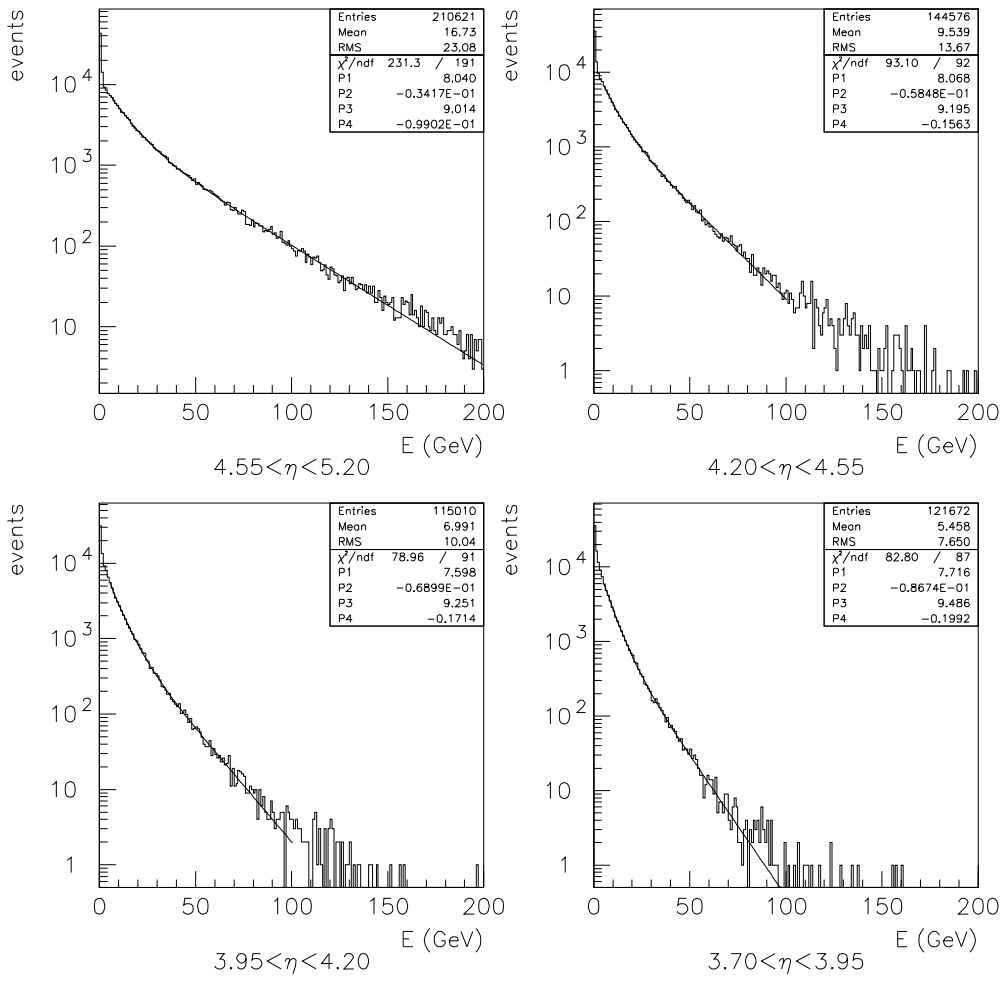

Figure 2: Particle energy deposited per tower in a ring. The line indicates the double exponential fit to the distribution.

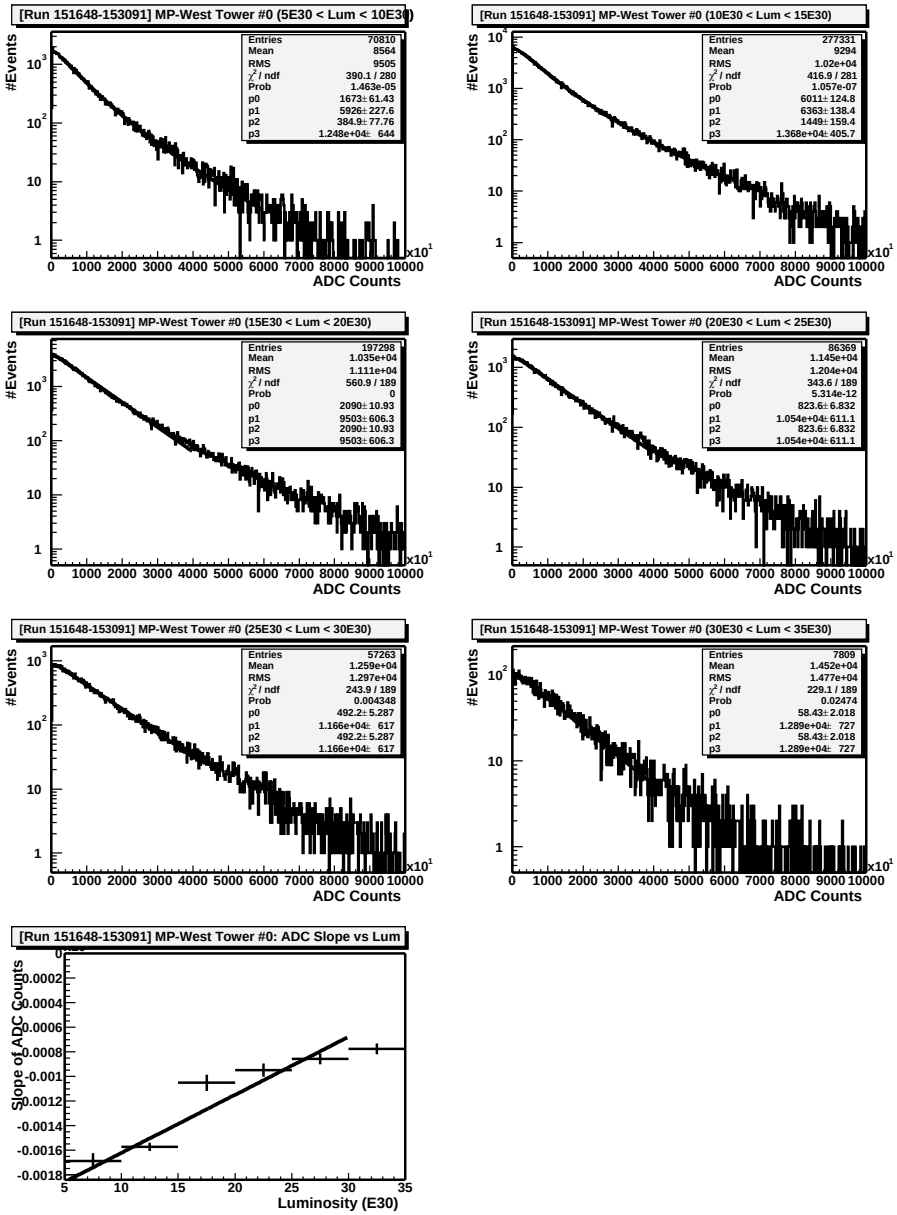

Figure 3: ADC count distributions of the West MiniPlug tower #0 in the inner layer for events with different luminosity intervals from 5E30 to 35E30 in the sample of runs 151648-153091. The curve in each plot is a double exponential fit to the distribution. First exponential slope of the fit as a function of luminosity (and a linear fit to it) is shown in the bottom-left plot.

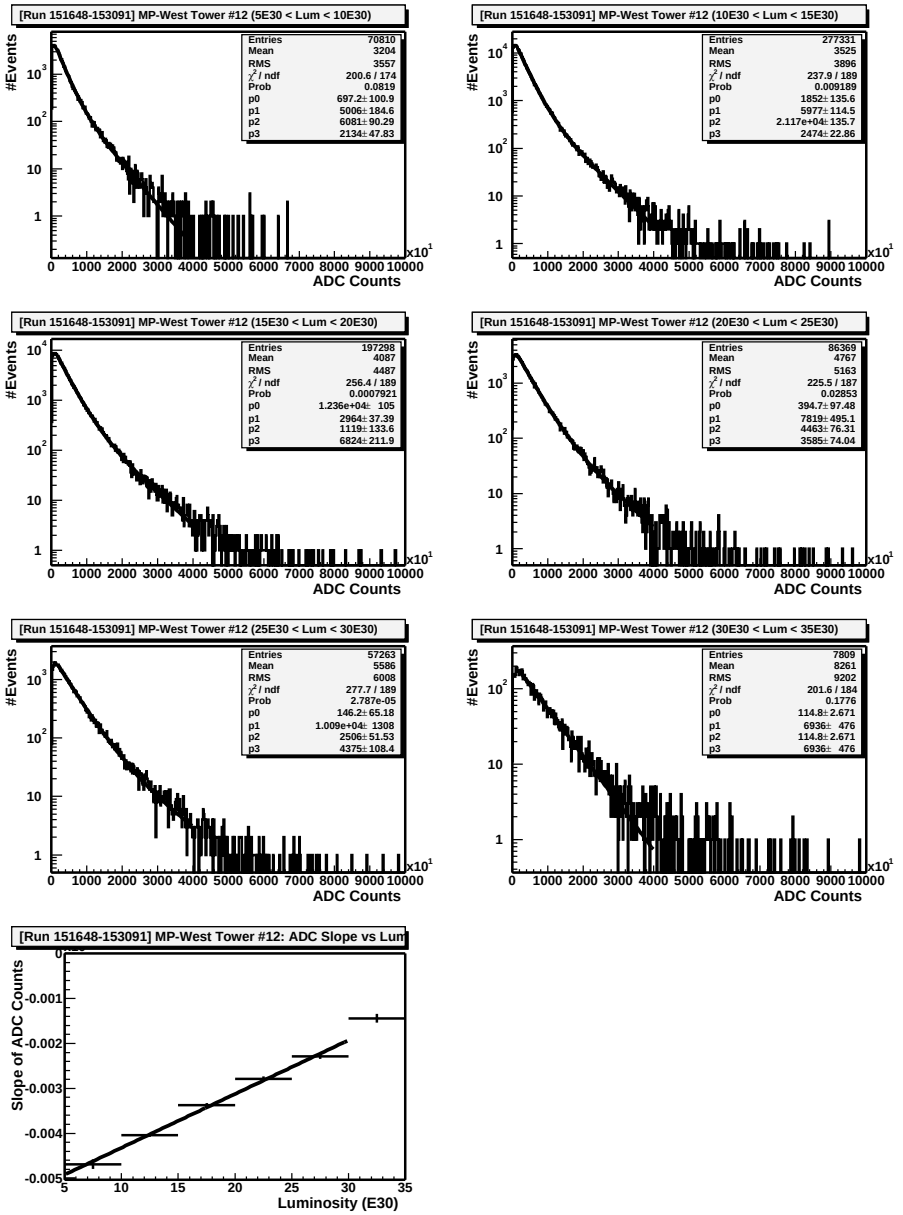

Figure 4: ADC count distributions of the West MiniPlug tower #12 in the outer layer for events with different luminosity intervals from 5E30 to 35E30 in the sample of runs 151648-153091. The curve in each plot is a double exponential fit to the distribution. First exponential slope of the fit as a function of luminosity (and a linear fit to it) is shown in the bottom-left plot.

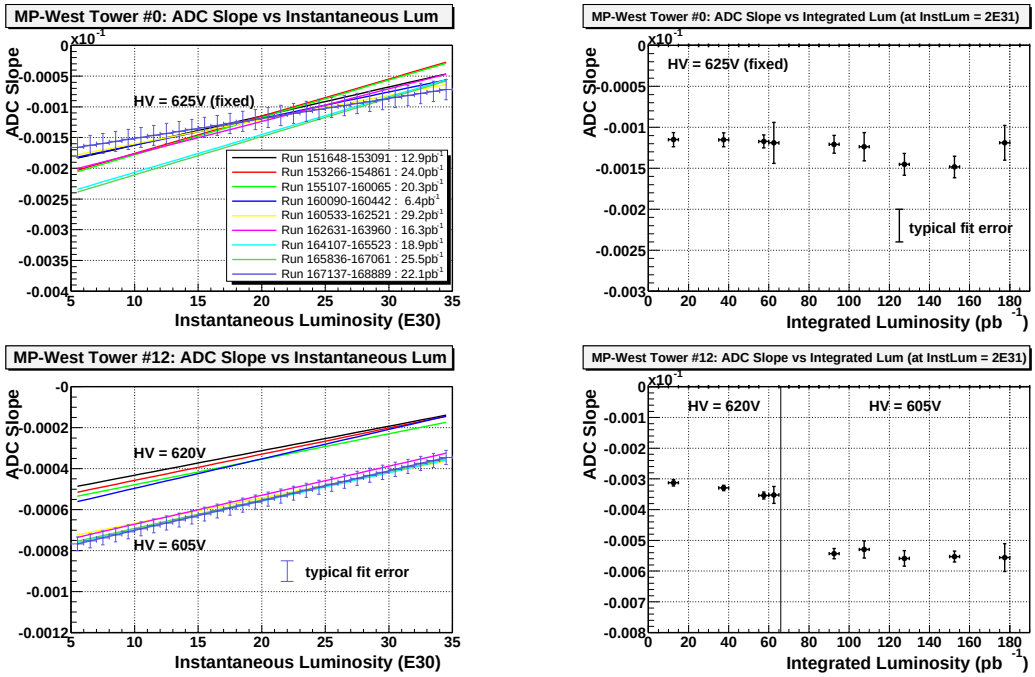

Figure 5: Fit results to the first exponential slope of double exponential fit (see in text) to ADC count distributions of the West MiniPlug tower #0 (top) and #12 (bottom). Left plots show the fits as a function of instantaneous luminosity, and right plots show the fits as a function of integrated luminosity at an instantaneous luminosity of 2E31.

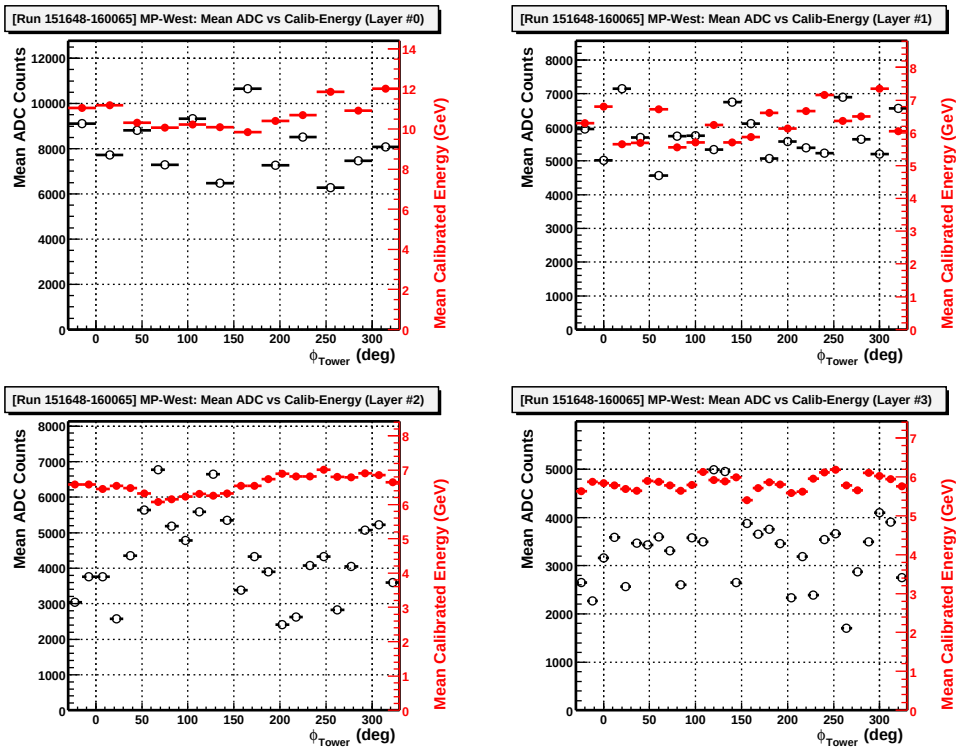

Figure 6: Mean values of raw ADC counts (open points) and Pass 1 calibrated energy (filled points) for West MiniPlug towers in each of four η-layers (top-left:layer #0, top-right:layer #1, bottom-left:layer #2, bottom-right:layer #3). The data is a minimum bias data selected with a requirement of 0 or 1 reconstructed vertex in runs 151638-153091.

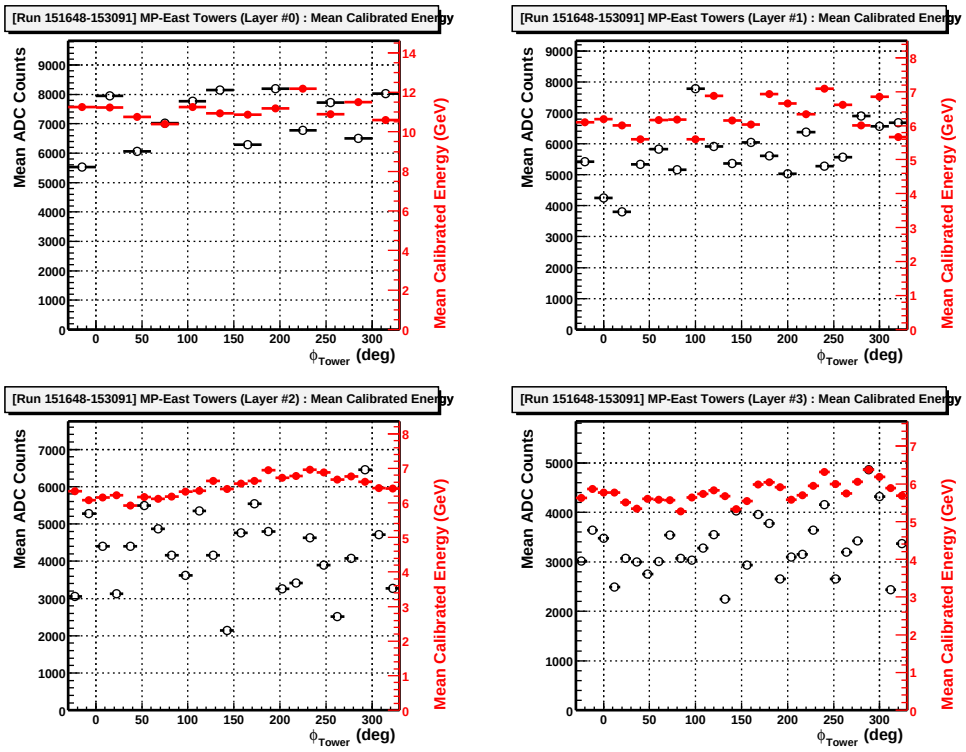

Figure 7: Mean values of raw ADC counts (open points) and Pass 1 calibrated energy (filled points) for East MiniPlug towers in each of four η-layers (top-left:layer #0, top-right:layer #1, bottom-left:layer #2, bottom-right:layer #3). The data is a minimum bias data selected with a requirement of 0 or 1 reconstructed vertex in runs 151638-153091.

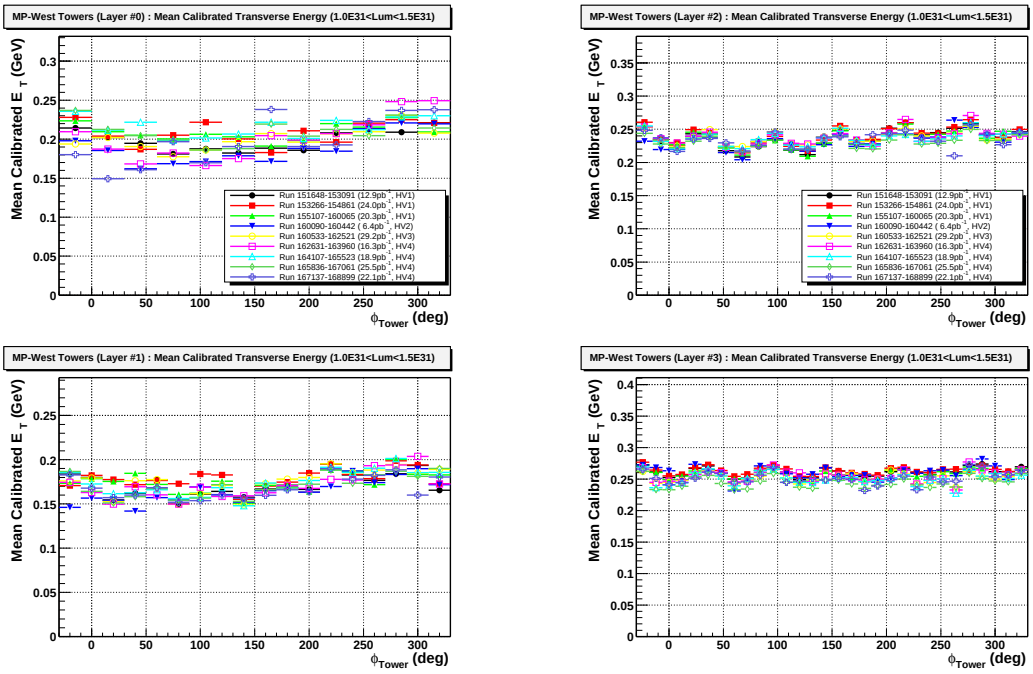

Figure 8: Mean values of Pass 1 calibrated transverse energy for West MiniPlug towers in each of four η-layers (top-left:layer #0, top-right:layer #1, bottom-left:layer #2, bottom-right:layer #3) at an instantaneous luminosity range of 1.0-1.5E31. The data is a minimum bias data selected with a requirement of 0 or 1 reconstructed vertex. Distributions for nine different run intervals are superimposed.

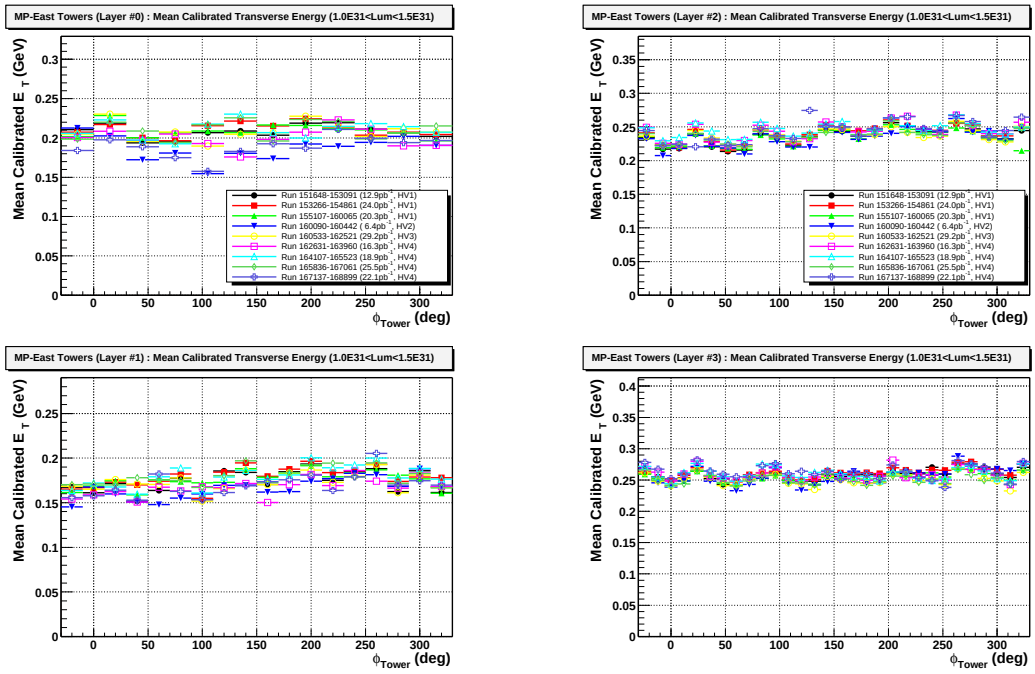

Figure 9: Mean values of Pass 1 calibrated transverse energy for East MiniPlug towers in each of four η-layers (top-left:layer #0, top-right:layer #1, bottom-left:layer #2, bottom-right:layer #3) at an instantaneous luminosity range of 1.0-1.5E31. The data is a minimum bias data selected with a requirement of 0 or 1 reconstructed vertex. Distributions for nine different run intervals are superimposed.

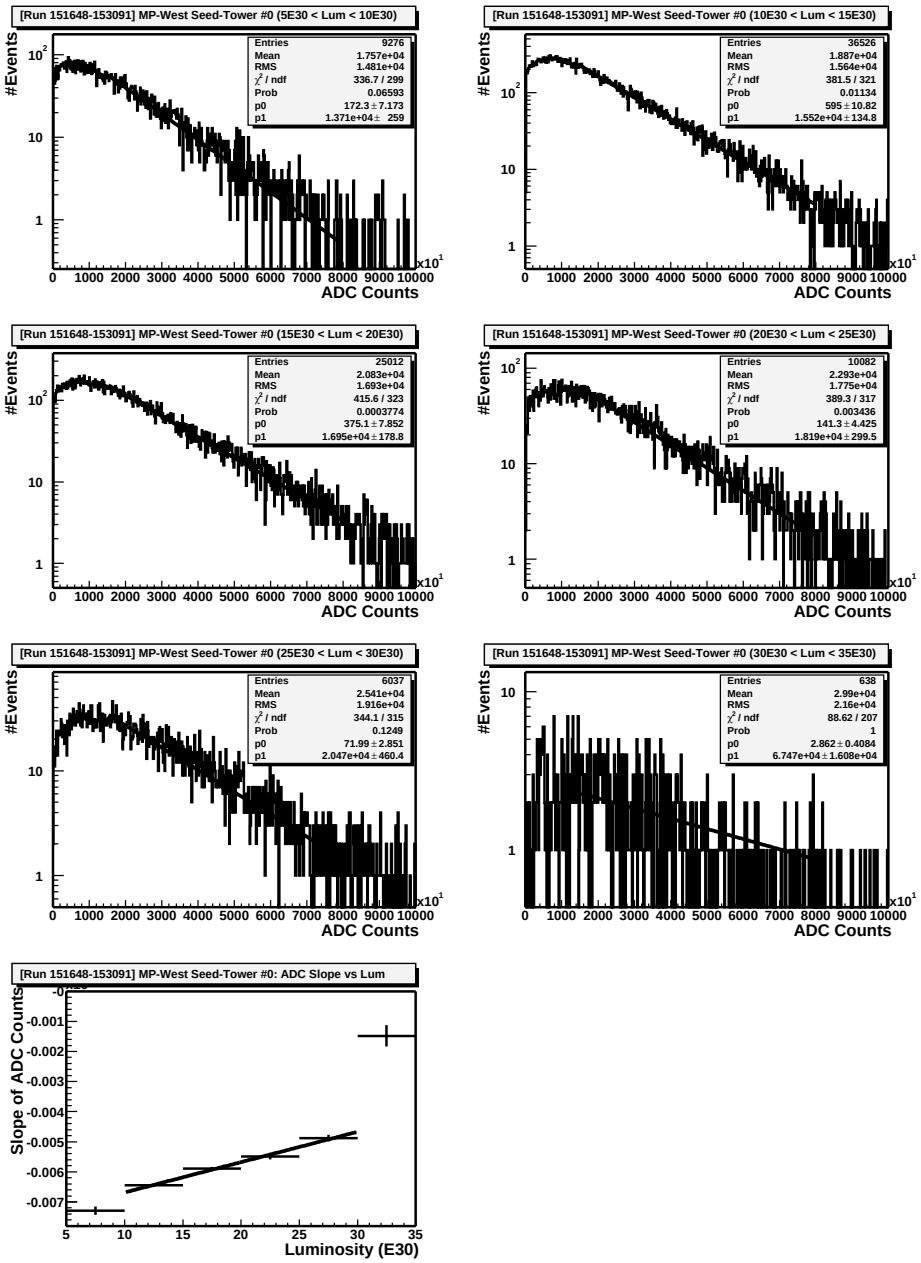

Figure 10: ADC count distributions of the West MiniPlug SEED tower #0 in the inner layer for events with different luminosity intervals from 5E30 to 35E30 in the sample of runs 151648-153091. The curve in each plot is a single exponential fit to the distribution. Exponential slope of the fit as a function of luminosity (and a linear fit to it) is shown in the bottom-left plot.

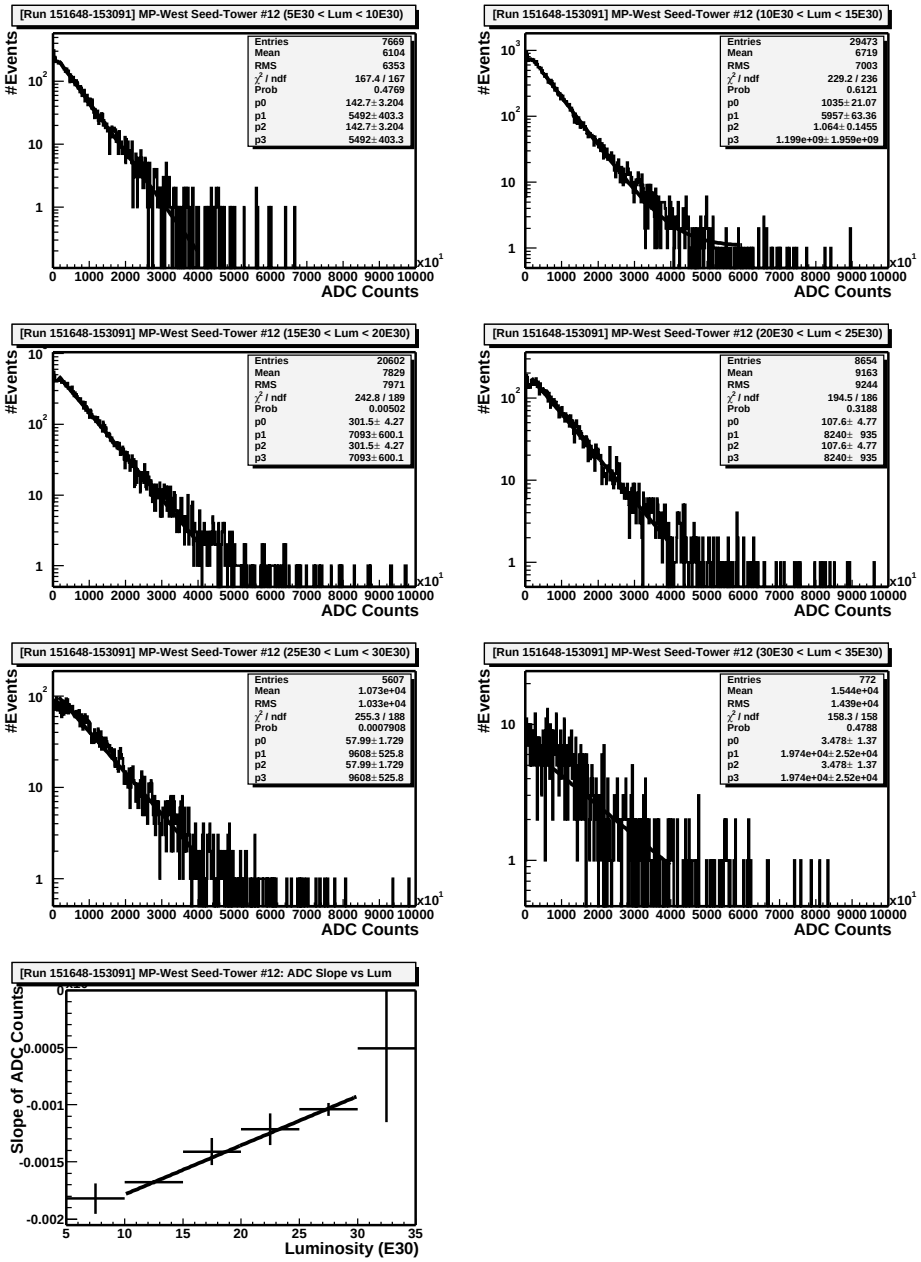

Figure 11: ADC count distributions of the West MiniPlug SEED tower #12 in the outer layer for events with different luminosity intervals from 5E30 to 35E30 in the sample of runs 151648-153091. The curve in each plot is a double exponential fit to the distribution. First exponential slope of the fit as a function of luminosity (and a linear fit to it) is shown in the bottom-left plot.

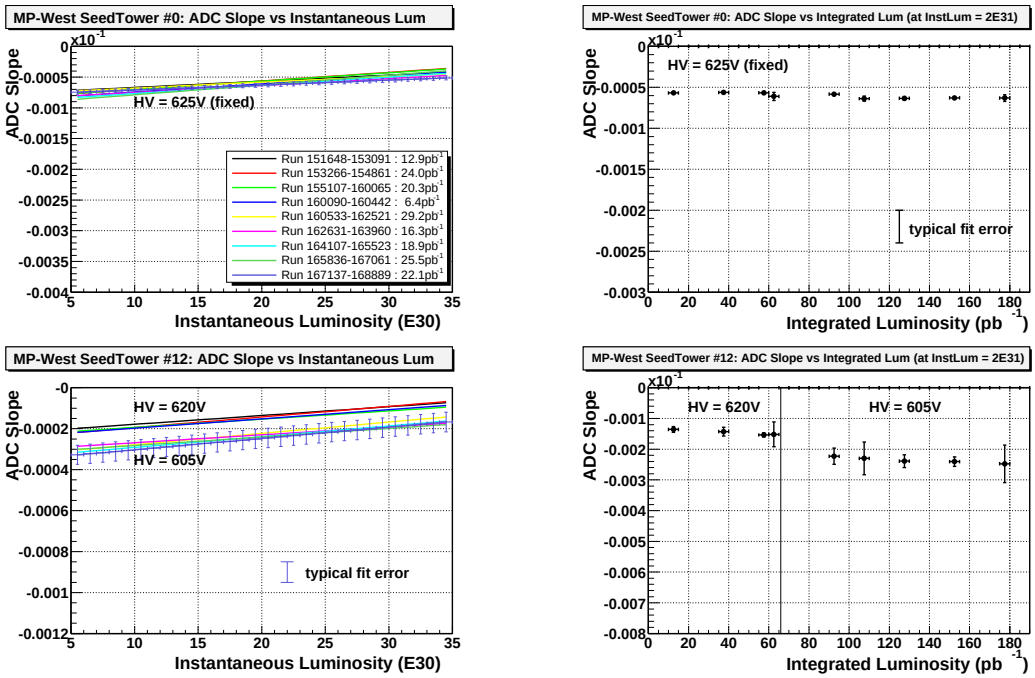

Figure 12: Fit results to the slope of exponential fit (see in text) to ADC count distributions of the West MiniPlug SEED tower #0 (top) and #12 (bottom). Left plots show the fits as a function of instantaneous luminosity, and right plots show the fits as a function of integrated luminosity at an instantaneous luminosity of 2E31.

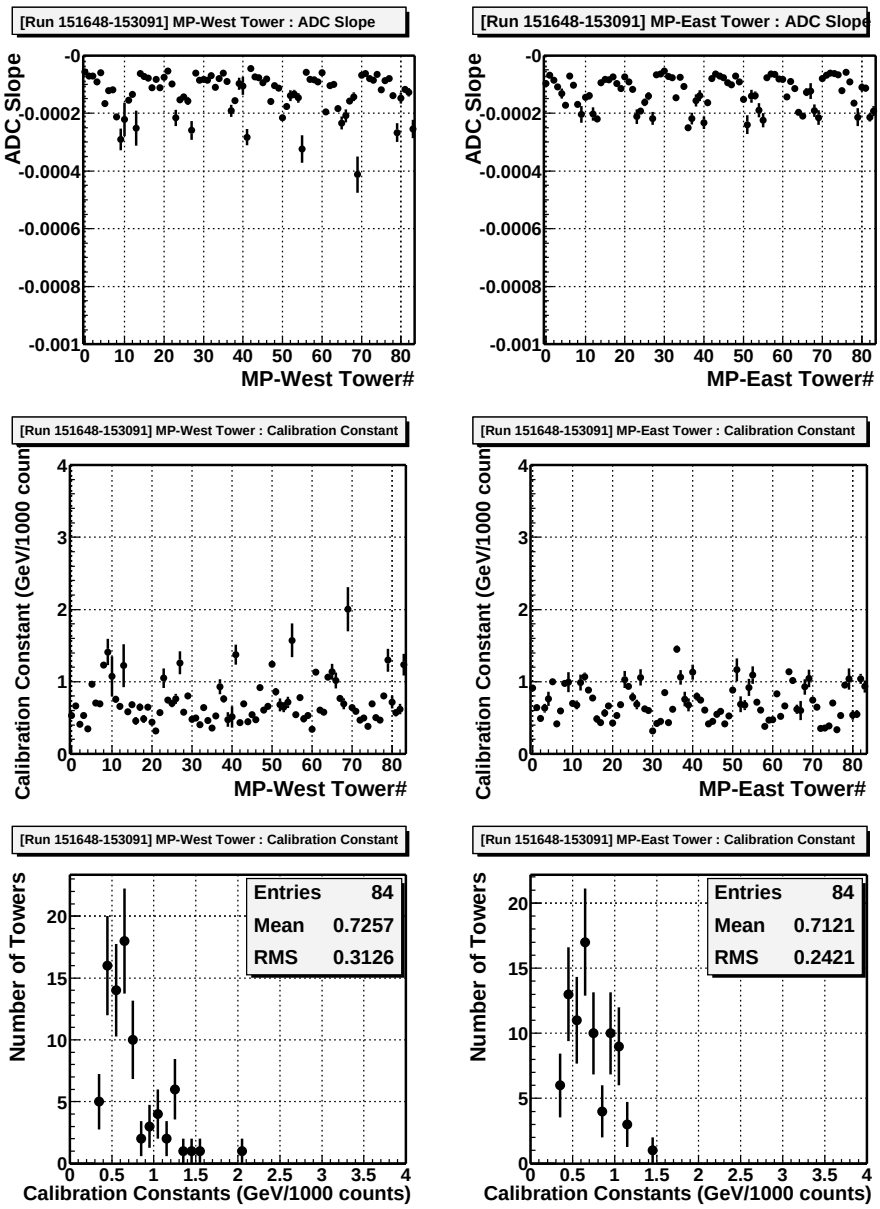

Figure 13: Slope of the exponential fit (top) and calibration constant (= energy in GeV per 1000 ADC counts) at a luminosity of 2E31 (middle) obtained from Pass 2 calibration versus tower number in runs 151648-153091. Bottom plots show the distributions of calibration constants for all towers. Left (right) side shows the distributions for the West (East) MiniPlug.

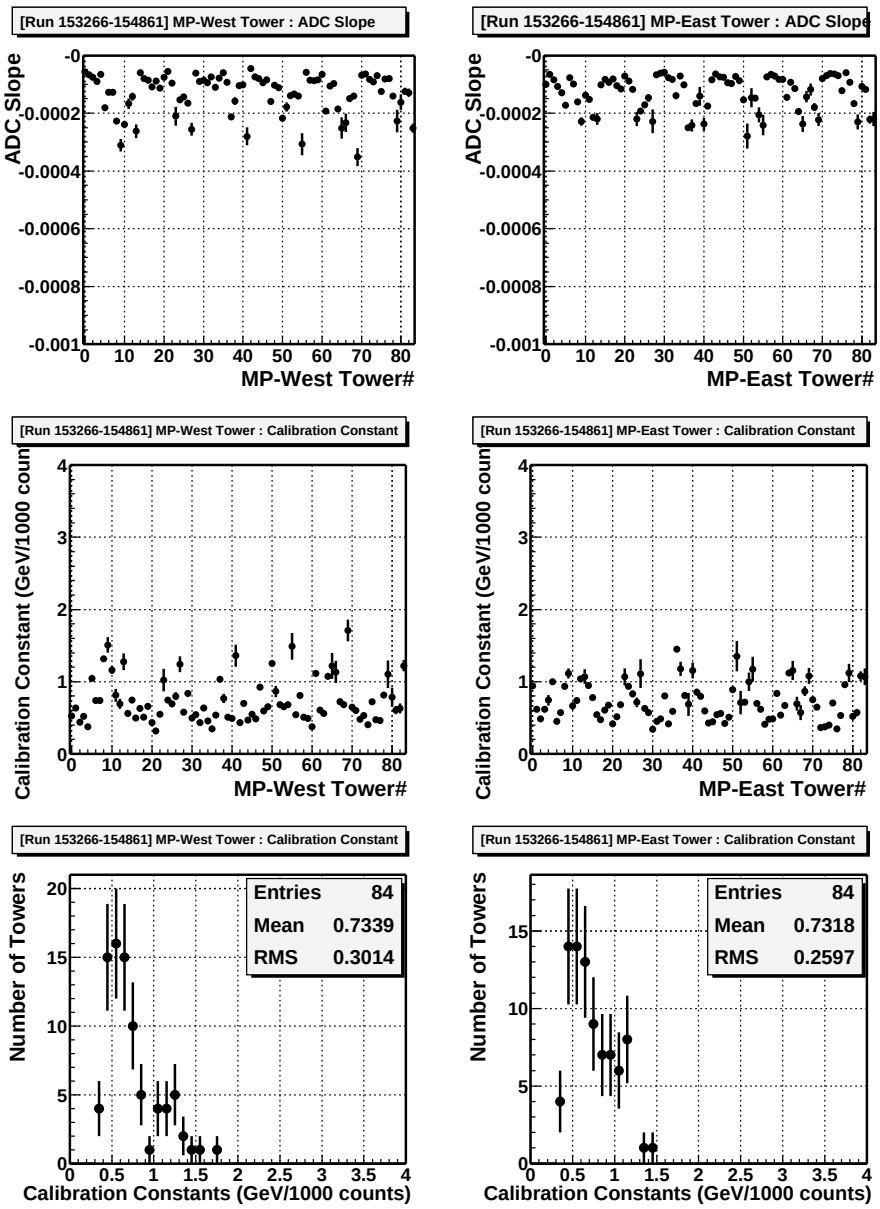

Figure 14: Slope of the exponential fit (top) and calibration constant (= energy in GeV per 1000 ADC counts) at a luminosity of 2E31 (middle) obtained from Pass 2 calibration versus tower number in runs 153266-154861. Bottom plots show the distributions of calibration constants for all towers. Left (right) side shows the distributions for the West (East) MiniPlug.

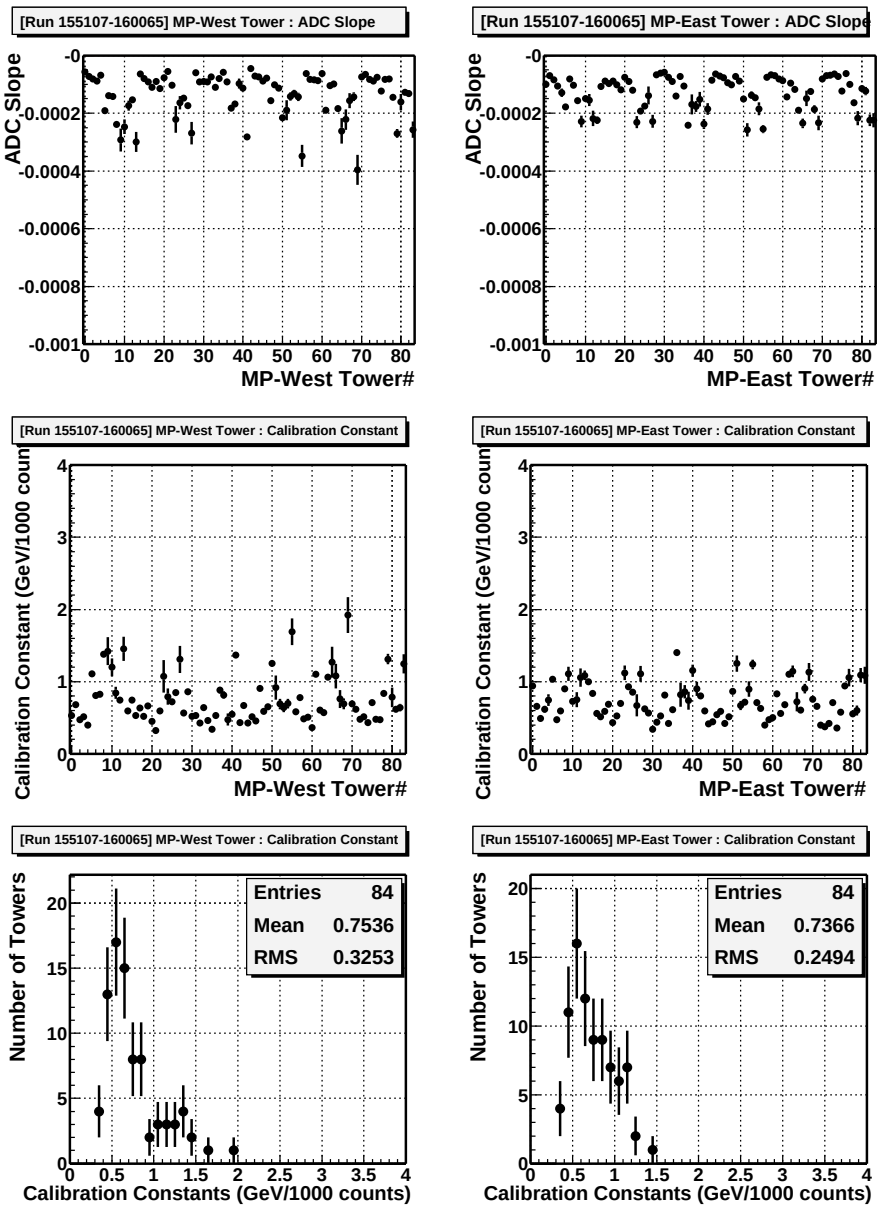

Figure 15: Slope of the exponential fit (top) and calibration constant (= energy in GeV per 1000 ADC counts) at a luminosity of 2E31 (middle) obtained from Pass 2 calibration versus tower number in runs 155107-160065. Bottom plots show the distributions of calibration constants for all towers. Left (right) side shows the distributions for the West (East) MiniPlug.

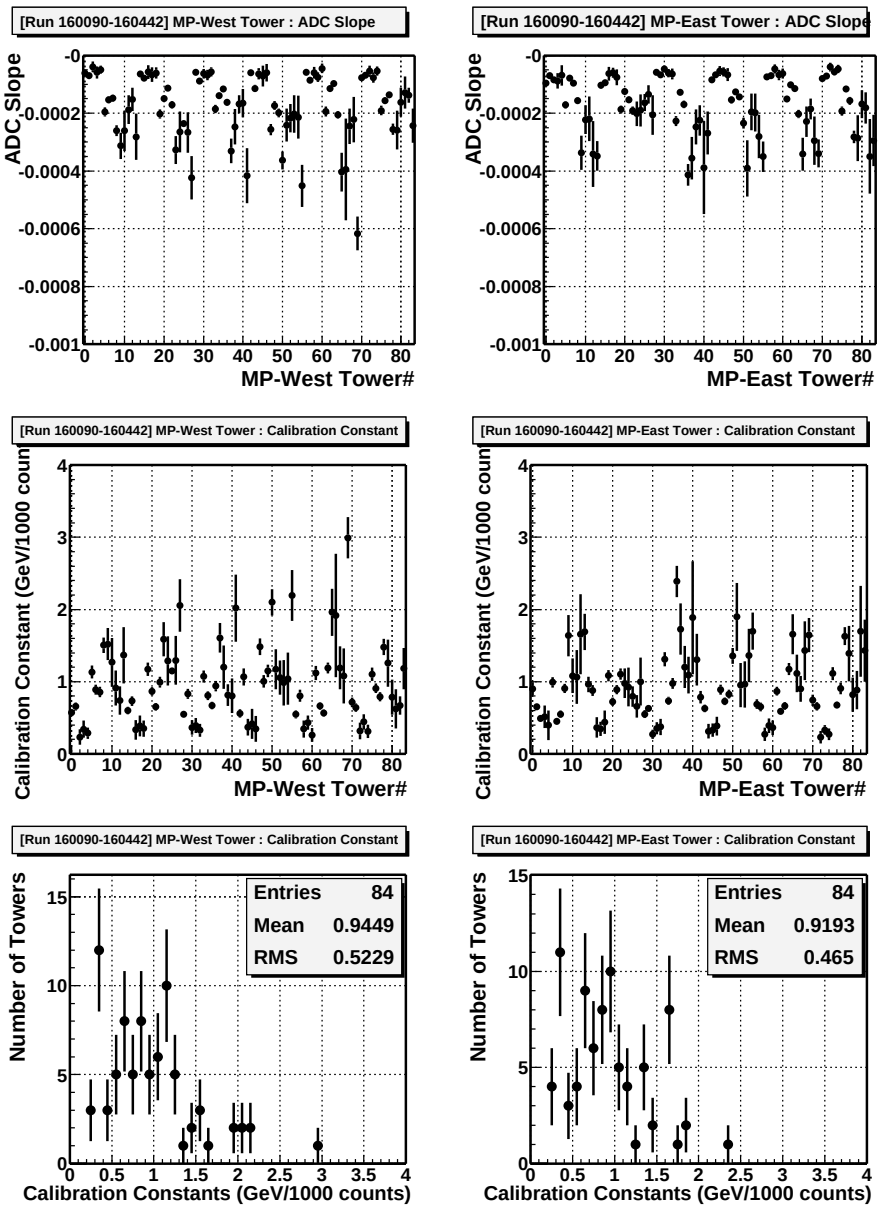

Figure 16: Slope of the exponential fit (top) and calibration constant (= energy in GeV per 1000 ADC counts) at a luminosity of 2E31 (middle) obtained from Pass 2 calibration versus tower number in runs 160090-160442. Bottom plots show the distributions of calibration constants for all towers. Left (right) side shows the distributions for the West (East) MiniPlug.

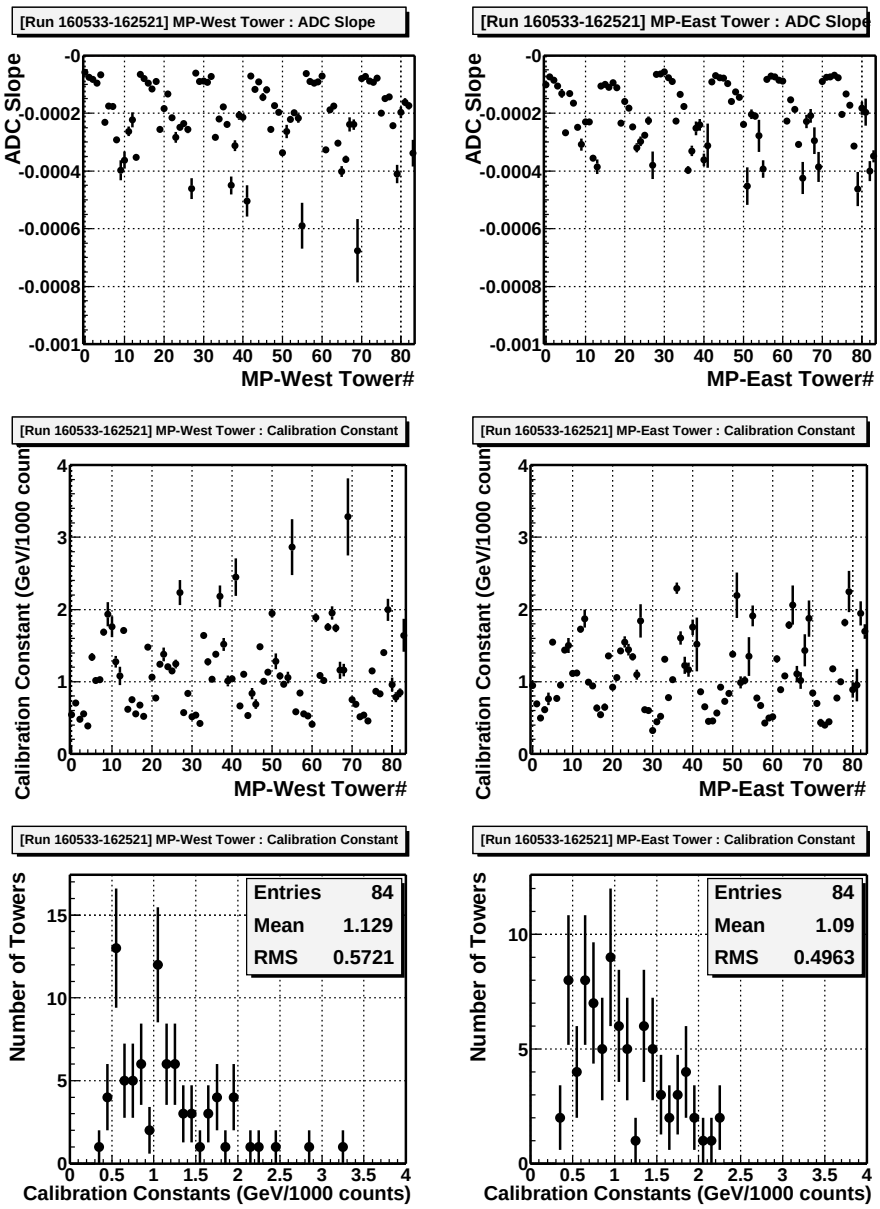

Figure 17: Slope of the exponential fit (top) and calibration constant (= energy in GeV per 1000 ADC counts) at a luminosity of 2E31 (middle) obtained from Pass 2 calibration versus tower number in runs 160533-162521. Bottom plots show the distributions of calibration constants for all towers. Left (right) side shows the distributions for the West (East) MiniPlug.

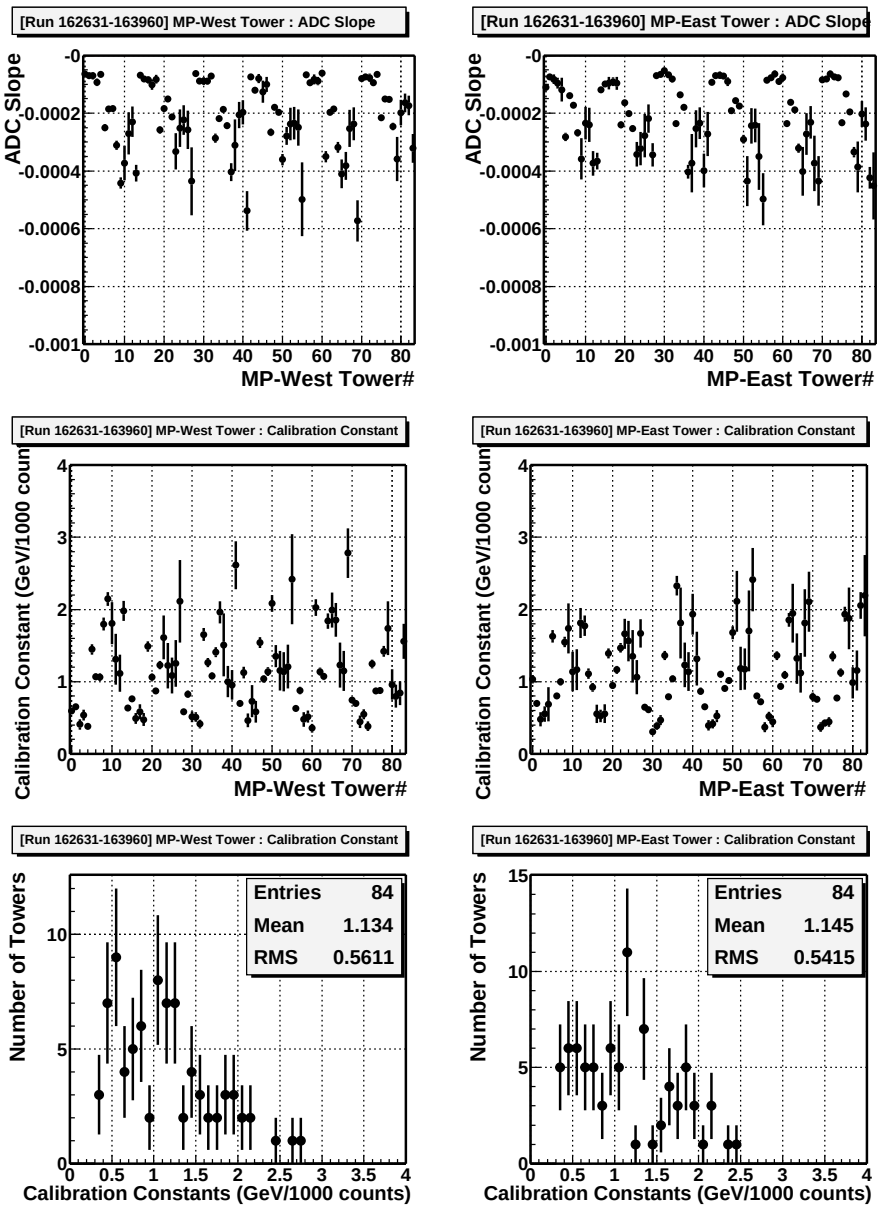

Figure 18: Slope of the exponential fit (top) and calibration constant (= energy in GeV per 1000 ADC counts) at a luminosity of 2E31 (middle) obtained from Pass 2 calibration versus tower number in runs 162631-163960. Bottom plots show the distributions of calibration constants for all towers. Left (right) side shows the distributions for the West (East) MiniPlug.

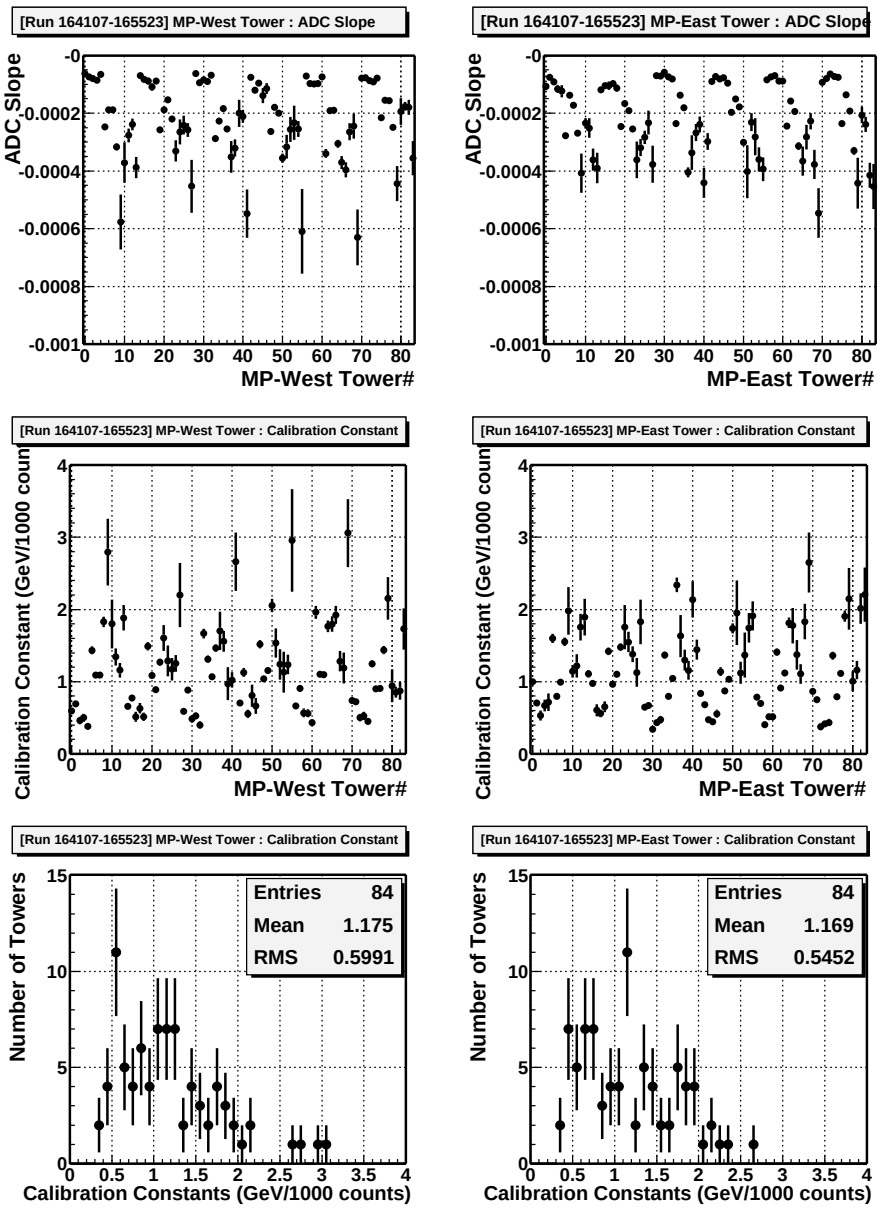

Figure 19: Slope of the exponential fit (top) and calibration constant (= energy in GeV per 1000 ADC counts) at a luminosity of 2E31 (middle) obtained from Pass 2 calibration versus tower number in runs 164107-165523. Bottom plots show the distributions of calibration constants for all towers. Left (right) side shows the distributions for the West (East) MiniPlug.

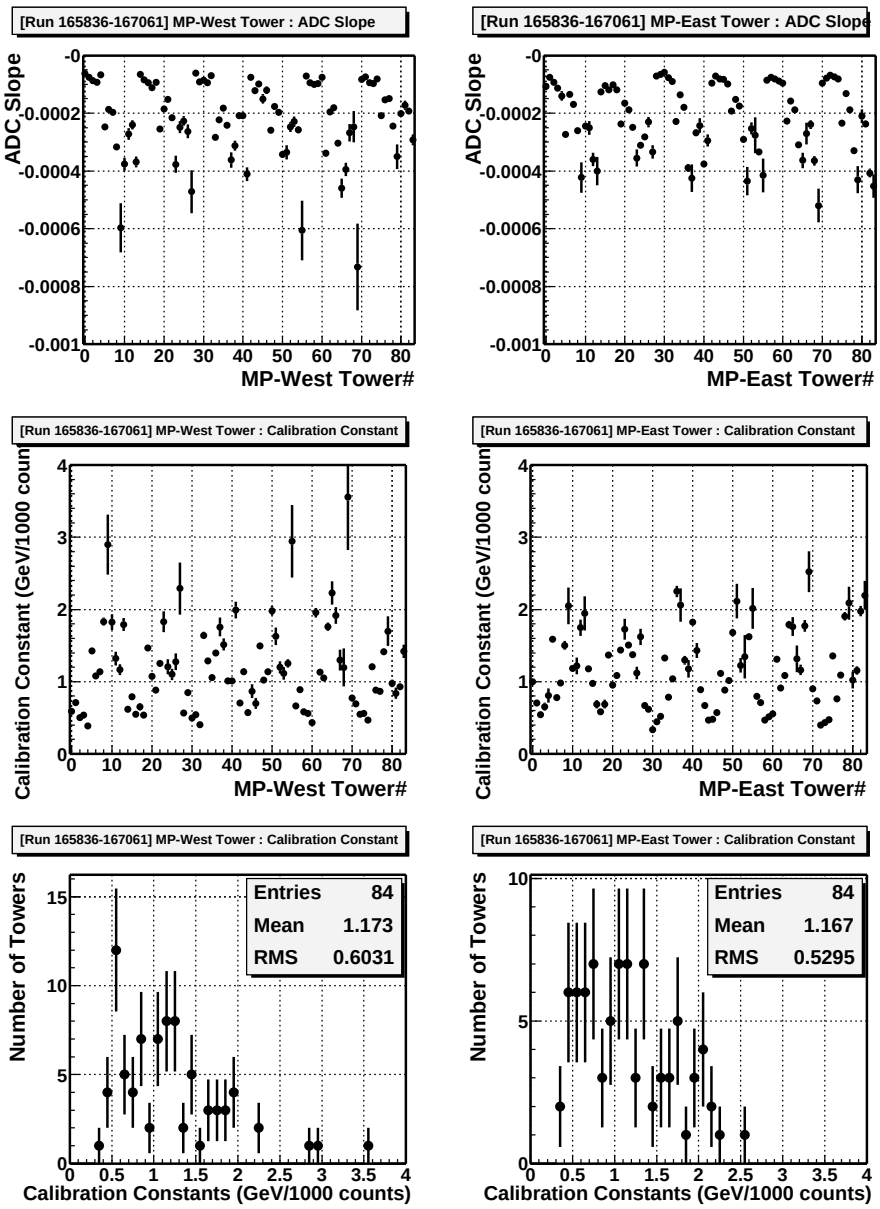

Figure 20: Slope of the exponential fit (top) and calibration constant (= energy in GeV per 1000 ADC counts) at a luminosity of 2E31 (middle) obtained from Pass 2 calibration versus tower number in runs 165836-167061. Bottom plots show the distributions of calibration constants for all towers. Left (right) side shows the distributions for the West (East) MiniPlug.

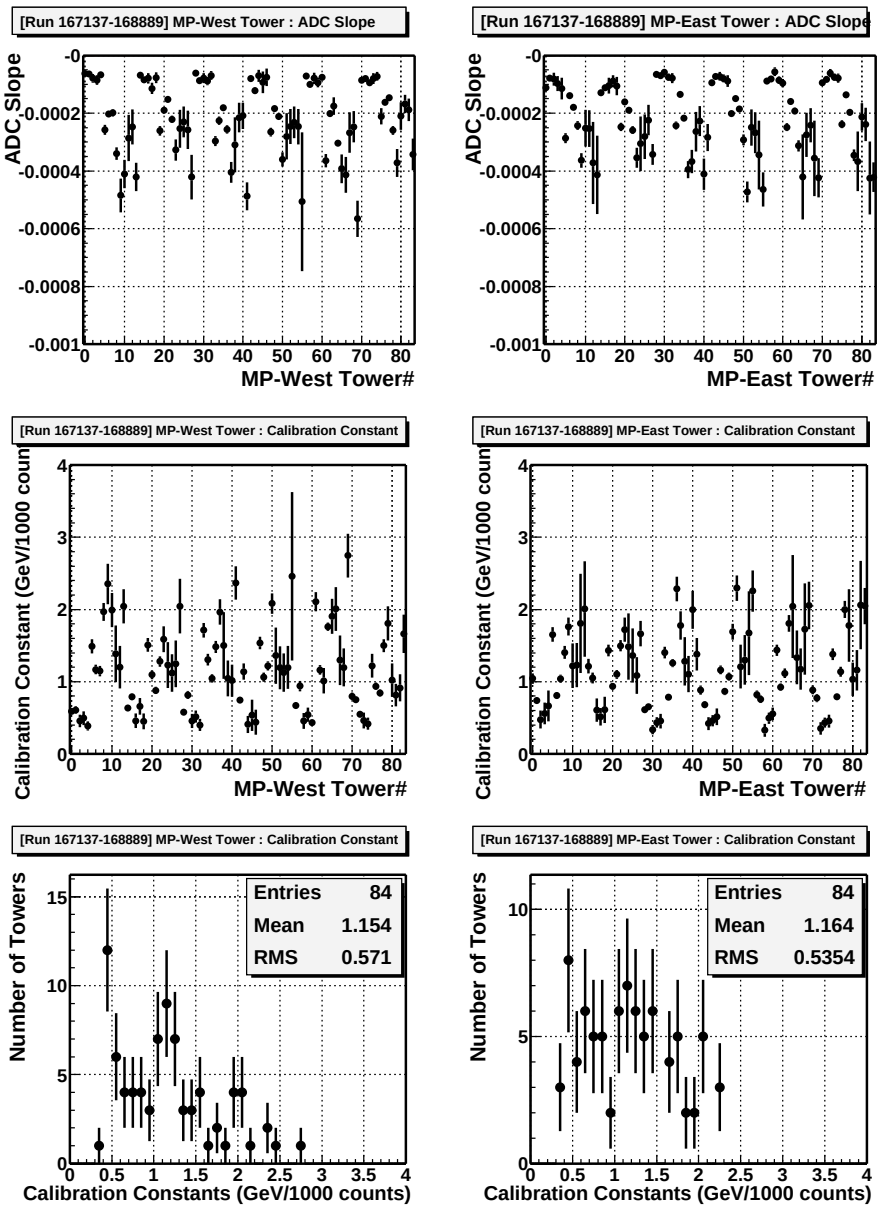

Figure 21: Slope of the exponential fit (top) and calibration constant (= energy in GeV per 1000 ADC counts) at a luminosity of 2E31 (middle) obtained from Pass 2 calibration versus tower number in runs 167137-168889. Bottom plots show the distributions of calibration constants for all towers. Left (right) side shows the distributions for the West (East) MiniPlug.

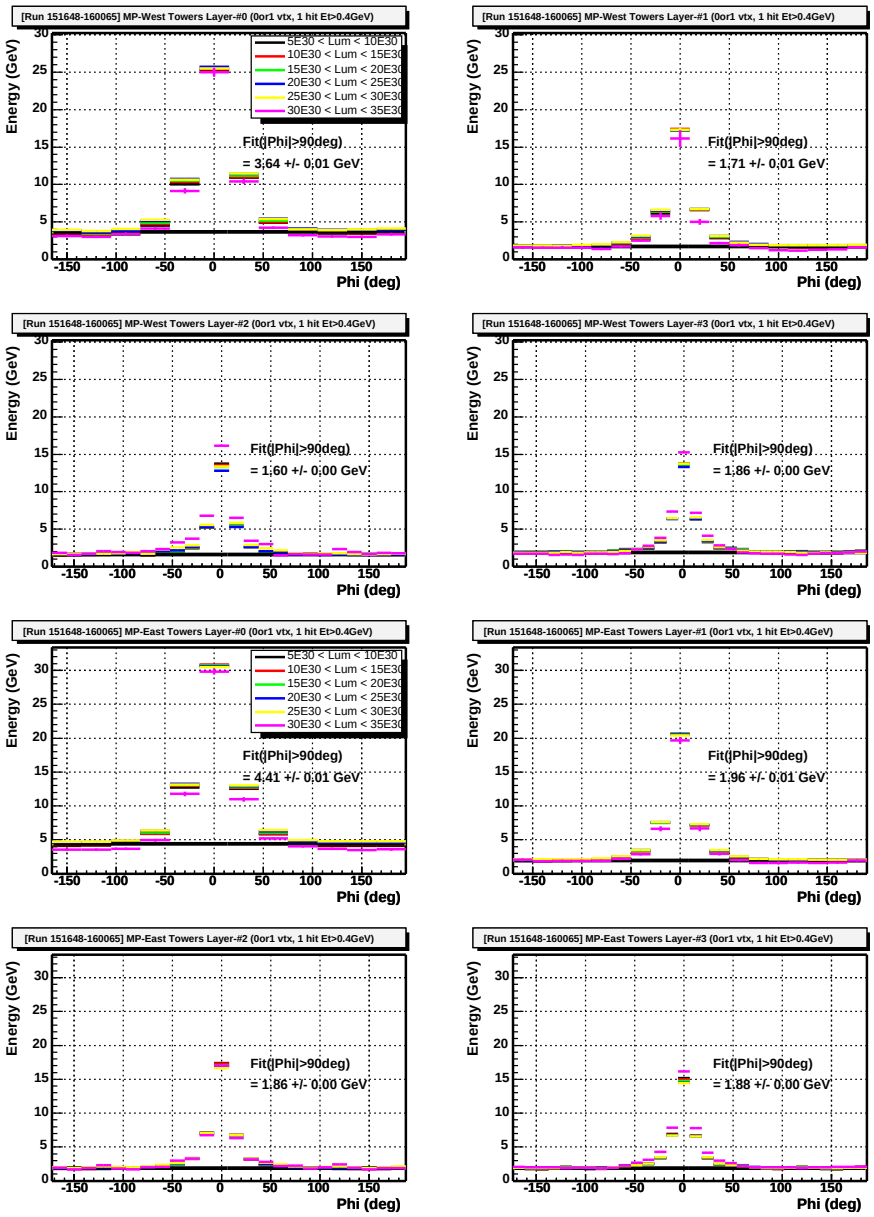

Figure 22: Top (bottom) four plots show the average energy of West (East) MiniPlug towers in each of four η-layers of the detector as a function of ϕ relative to the seed tower which is always positioned at $\phi = 0$. The seed tower is required to have $E_T > 400$ MeV and to be only one in a detector. The average energy of towers in a layer which the seed tower belongs to is plotted. The distributions for six different luminosity intervals are superimposed. The straight line and a number in each plot show the level of flat energy obtained at $|\phi| > 90°$.

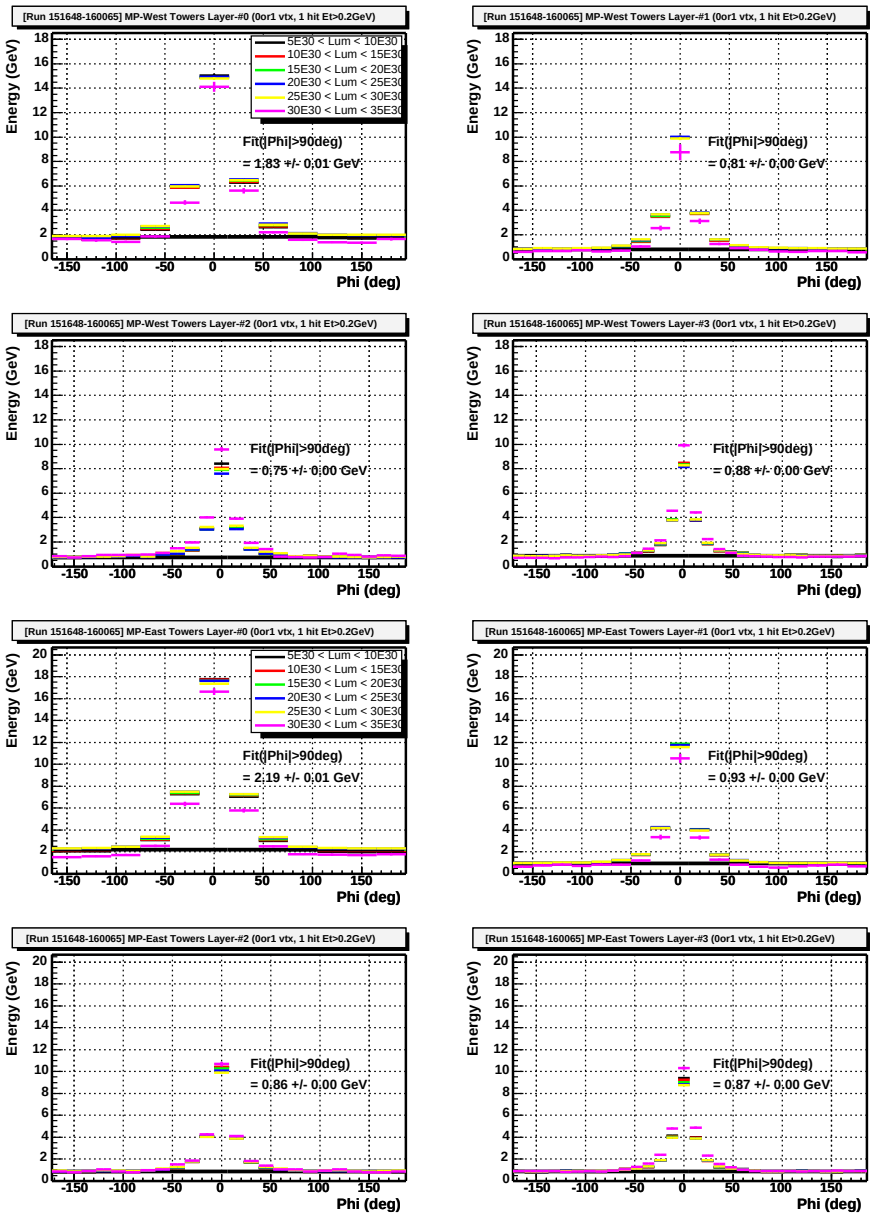

Figure 23: Top (bottom) four plots show the average energy of West (East) MiniPlug towers in each of four η-layers of the detector as a function of ϕ relative to the seed tower which is always positioned at $\phi = 0$. The seed tower is required to have $E_T > 200$ MeV and to be only one in a detector. The average energy of towers in a layer which the seed tower belongs to is plotted. The distributions for six different luminosity intervals are superimposed. The straight line and a number in each plot show the level of flat energy obtained at $|\phi| > 90°$.

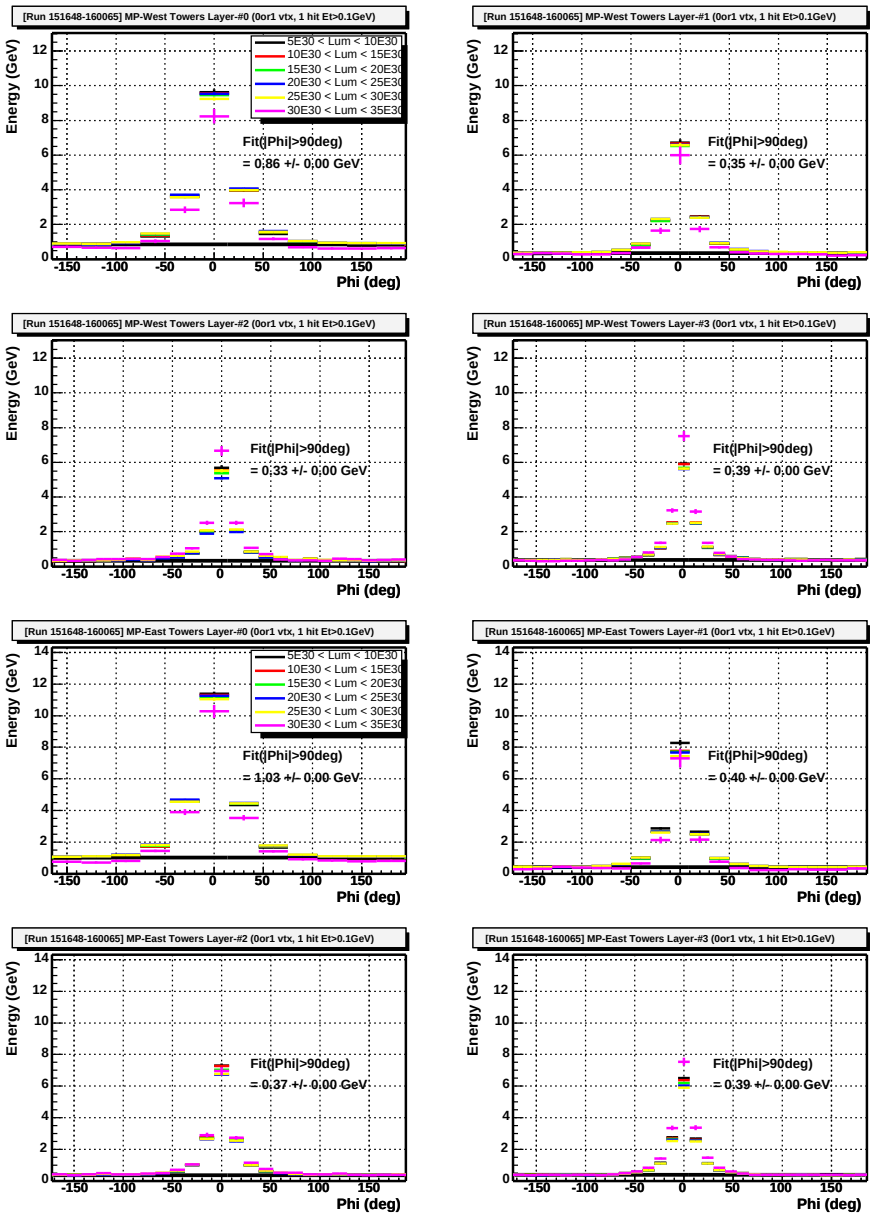

Figure 24: Top (bottom) four plots show the average energy of West (East) MiniPlug towers in each of four η-layers of the detector as a function of ϕ relative to the seed tower which is always positioned at $\phi = 0$. The seed tower is required to have $E_T > 100$ MeV and to be only one in a detector. The average energy of towers in a layer which the seed tower belongs to is plotted. The distributions for six different luminosity intervals are superimposed. The straight line and a number in each plot show the level of flat energy obtained at $|\phi| > 90°$.

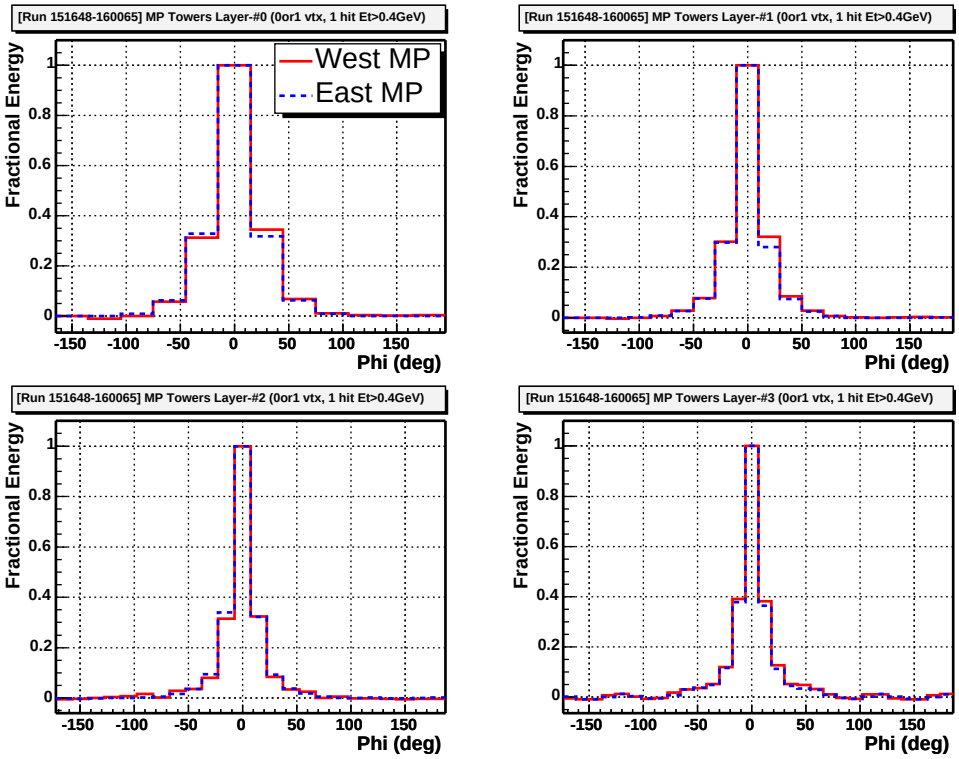

Figure 25: Fractional energy of MiniPlug towers in each of four η-layers of the detector with respect to the energy of seed tower which is always positioned at $\phi = 0$. The solid (dashed) histograms show the distributions for West (East) MiniPlug. The seed tower is required to have $E_T > 400$ MeV and to be only one in a detector. The average energy of towers in a layer which the seed tower belongs to is plotted.

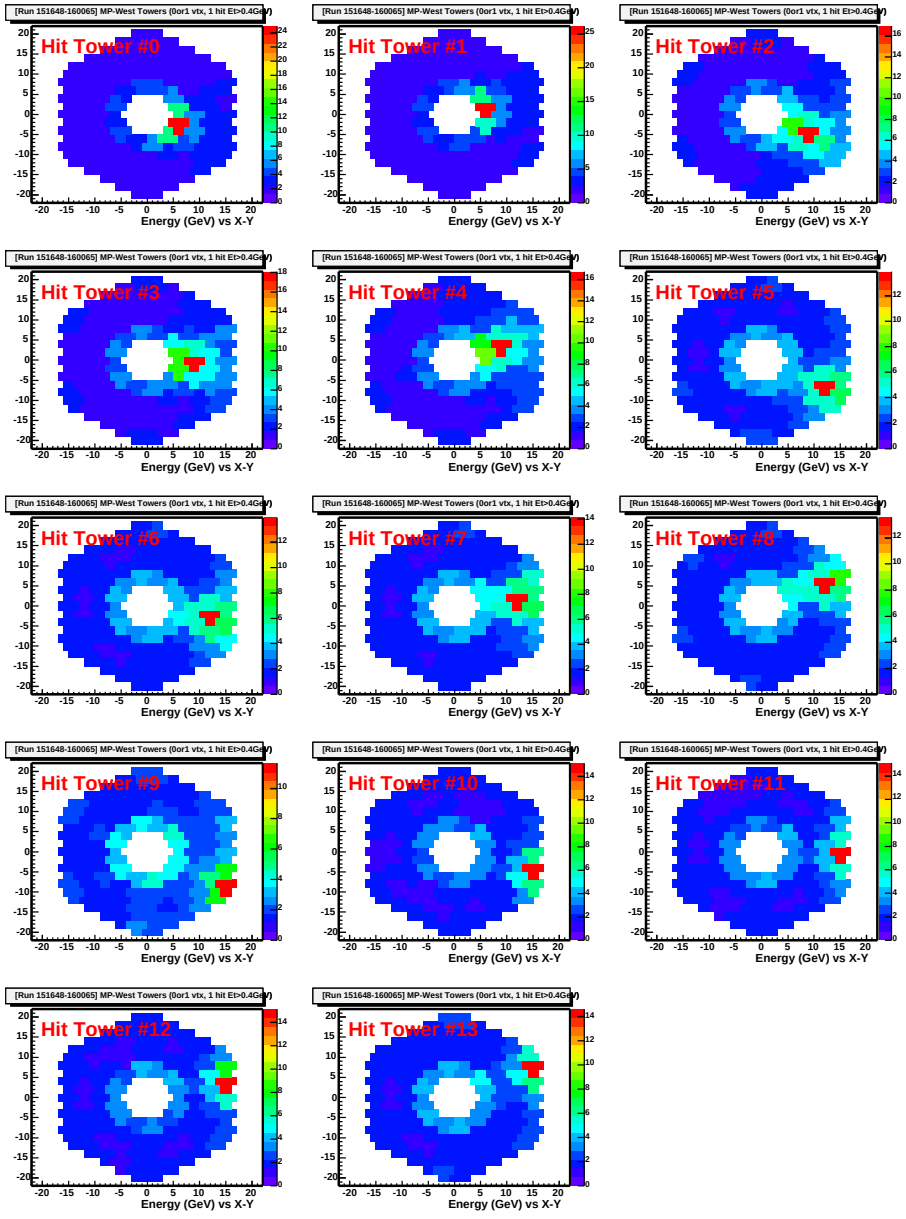

Figure 26: Average energy of West MiniPlug towers shown in two dimensional (X-Y) plane perpendicular to the beam for events with only one seed tower which is positioned at a location denoted in each plot. The seed tower is required to have $E_T > 400$ MeV.

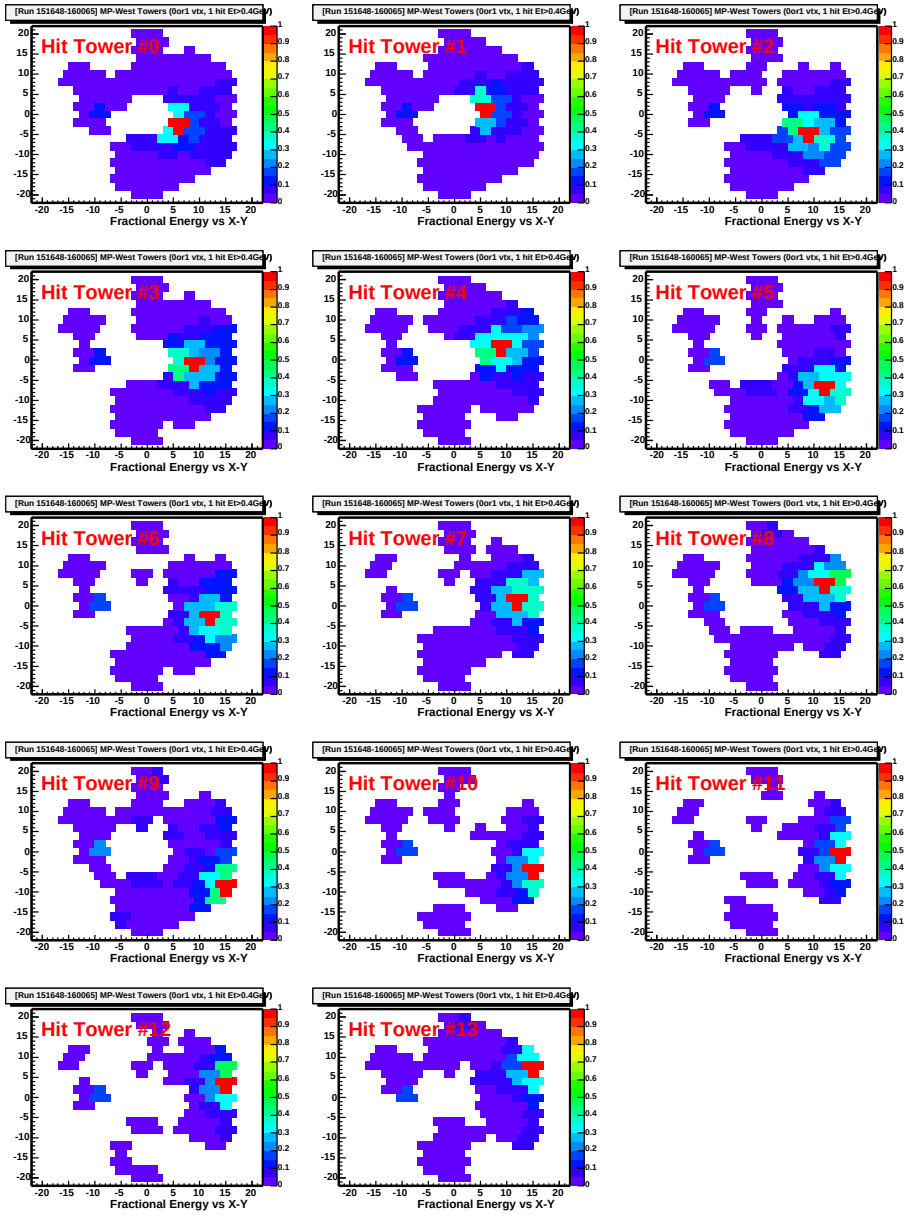

Figure 27: Fractional energy of West MiniPlug towers with respect to the energy of seed tower for events with only one seed tower which is positioned at a location denoted in each plot. The seed tower is required to have $E_T > 400$ MeV.

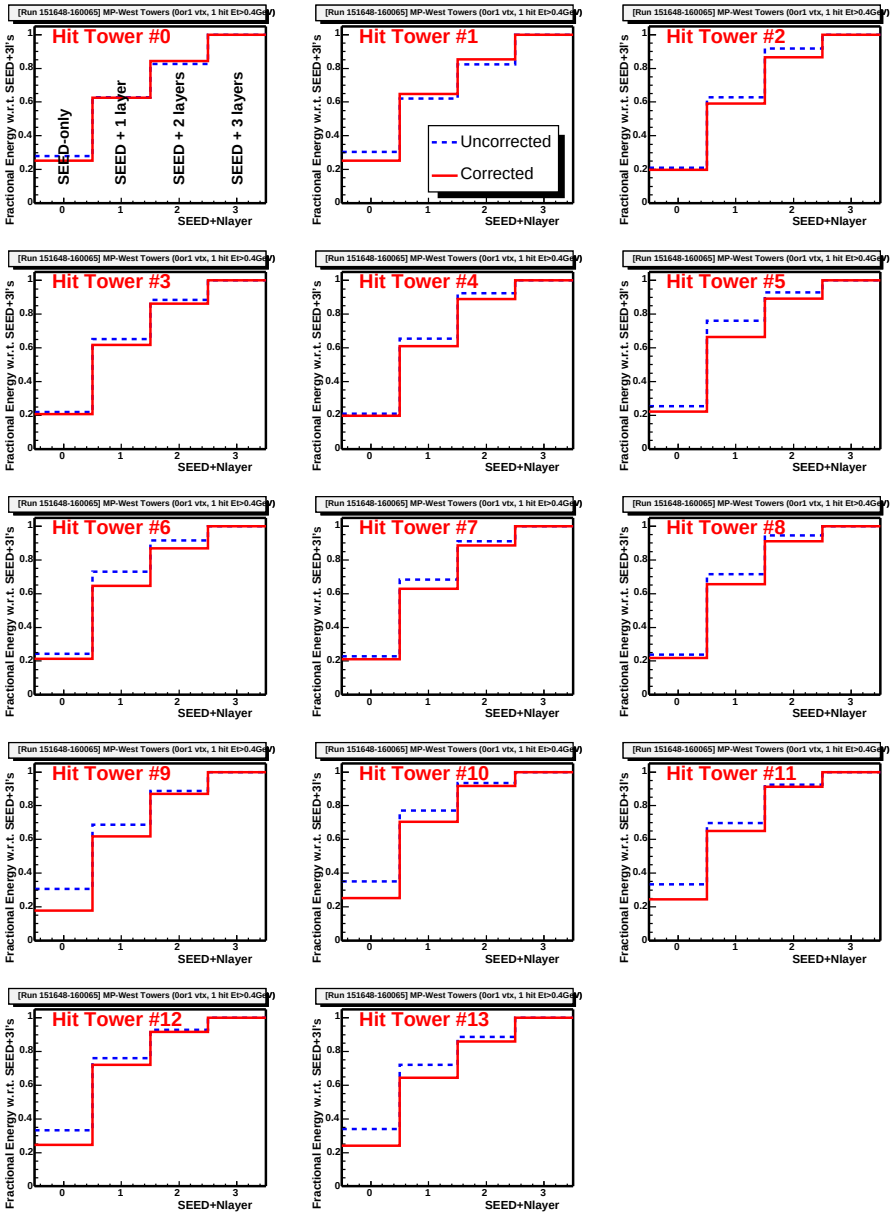

Figure 28: Average energy deposited in a seed plus adjacent towers in zero, one, two and three concentric layers for West MiniPlug. The energy is normalized to the 4th bin (seed plus three concentric towers). The seed tower is required to have $E_T > 400$ MeV. Distributions labeled "uncorrected" are obtained from measured energy in the detector, while the ones labeled "corrected" are obtained from energy corrected for particle energy loss described in the text.

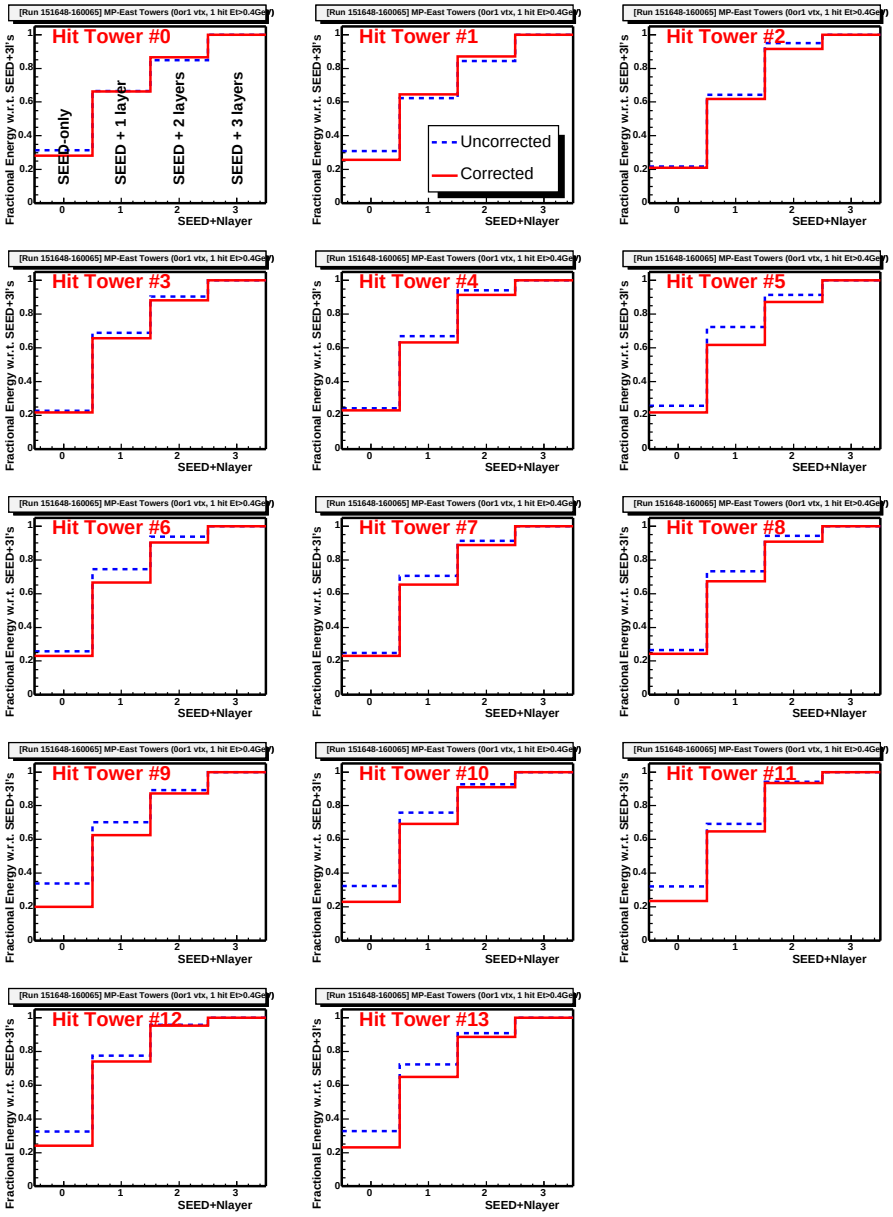

Figure 29: Average energy deposited in a seed plus adjacent towers in zero, one, two and three concentric layers for East MiniPlug. The energy is normalized to the 4th bin (seed plus three concentric towers). The seed tower is required to have $E_T > 400$ MeV. Distributions labeled "uncorrected" are obtained from measured energy in the detector, while the ones labeled "corrected" are obtained from energy corrected for particle energy loss described in the text.

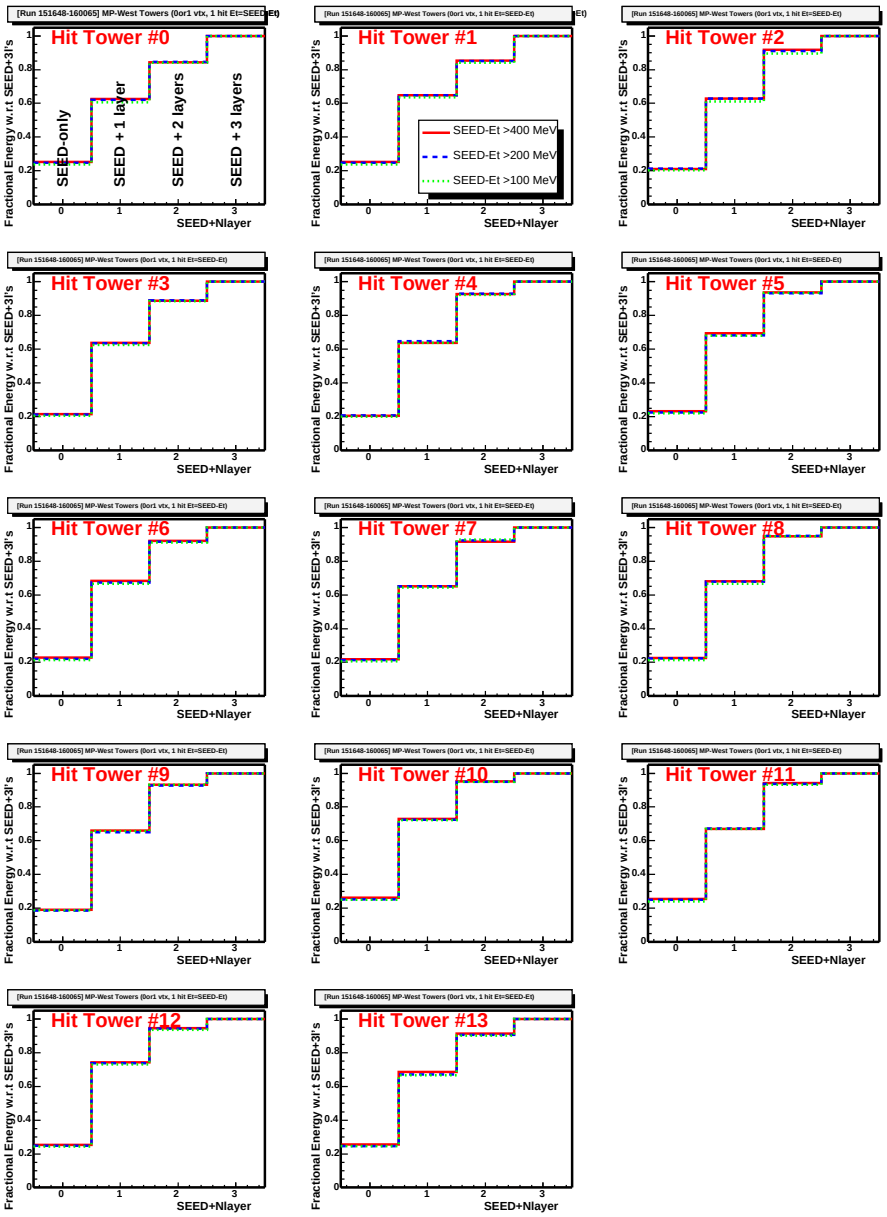

Figure 30: Average "corrected" energy deposited in a seed plus adjacent towers in zero, one, two and three concentric layers for West MiniPlug. The energy is normalized to the 4th bin (seed plus three concentric towers). Three histograms in each plot correspond to the seed tower with $E_T > 400$ MeV (solid), $E_T > 200$ MeV (dashed) and $E_T > 100$ MeV (dotted).

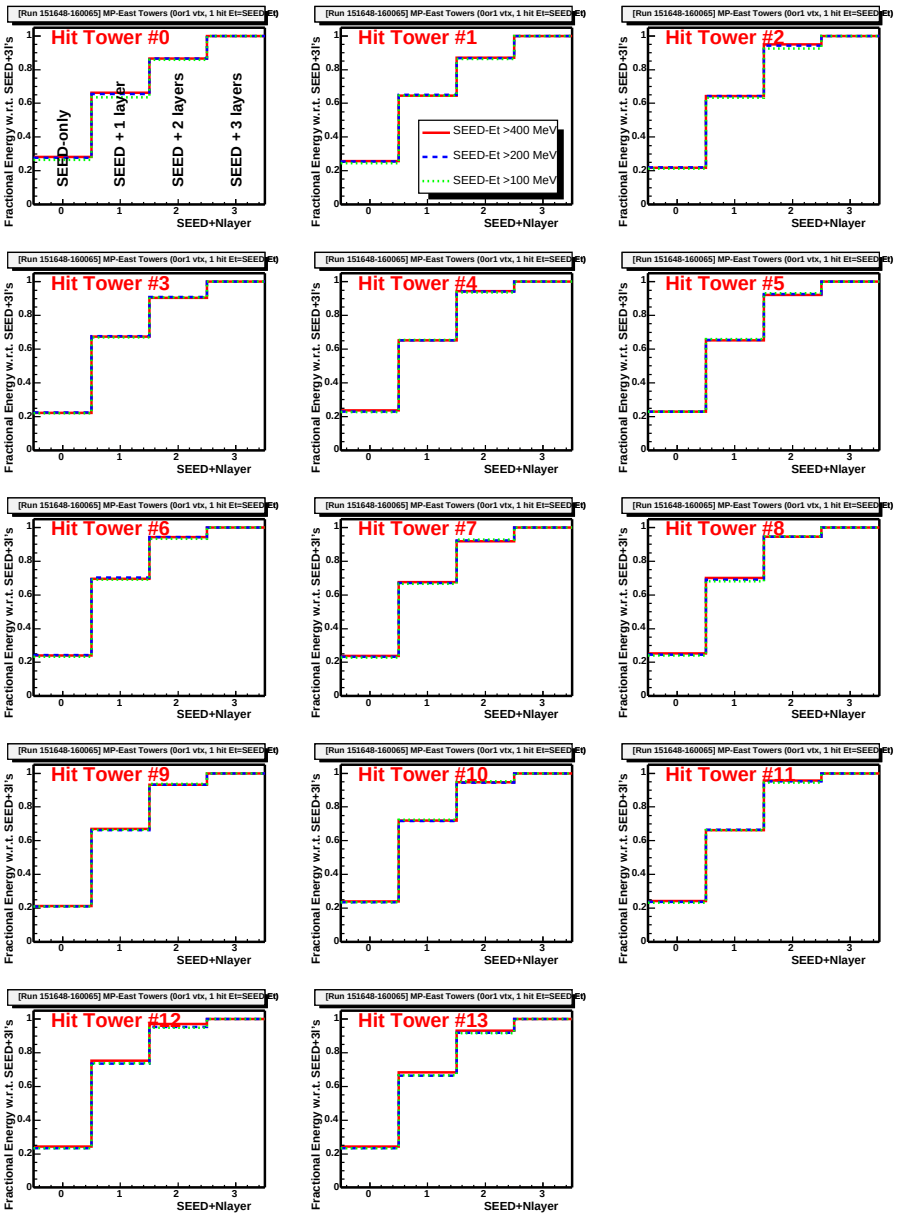

Figure 31: Average "corrected" energy deposited in a seed plus adjacent towers in zero, one, two and three concentric layers for East MiniPlug. The energy is normalized to the 4th bin (seed plus three concentric towers). Three histograms in each plot correspond to the seed tower with $E_T > 400$ MeV (solid), $E_T > 200$ MeV (dashed) and $E_T > 100$ MeV (dotted).

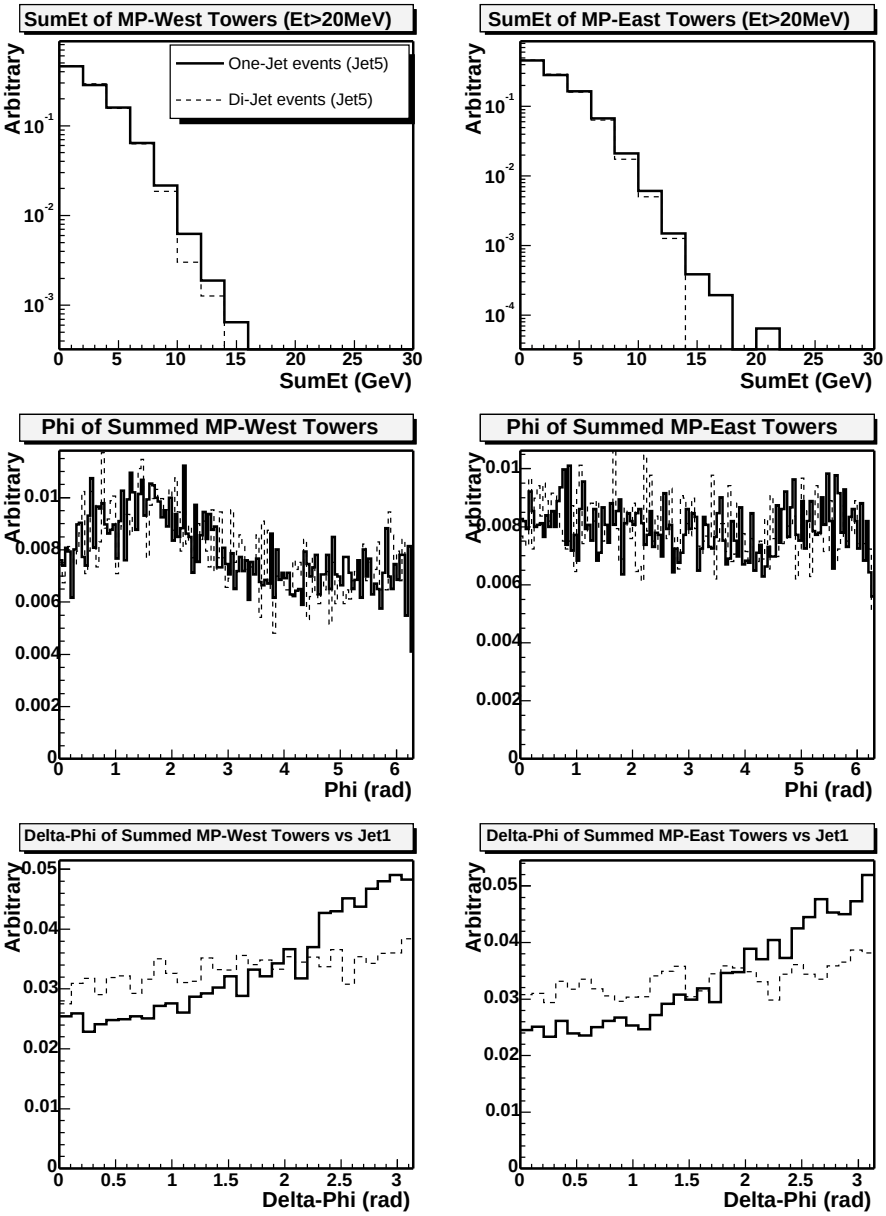

Figure 32: Scaler E_T sum of MiniPlug towers with $E_T > 20$ MeV (top), azimuthal angle of (vector) sum of MiniPlug towers (middle) and the difference of azimuthal angle between the miniplug jet and the leading jet in the central calorimeter (bottom). The solid (dashed) lines show distributions for one-jet (di-jet) events. The distributions for the West (East) MiniPlug are shown in the left (right) side.

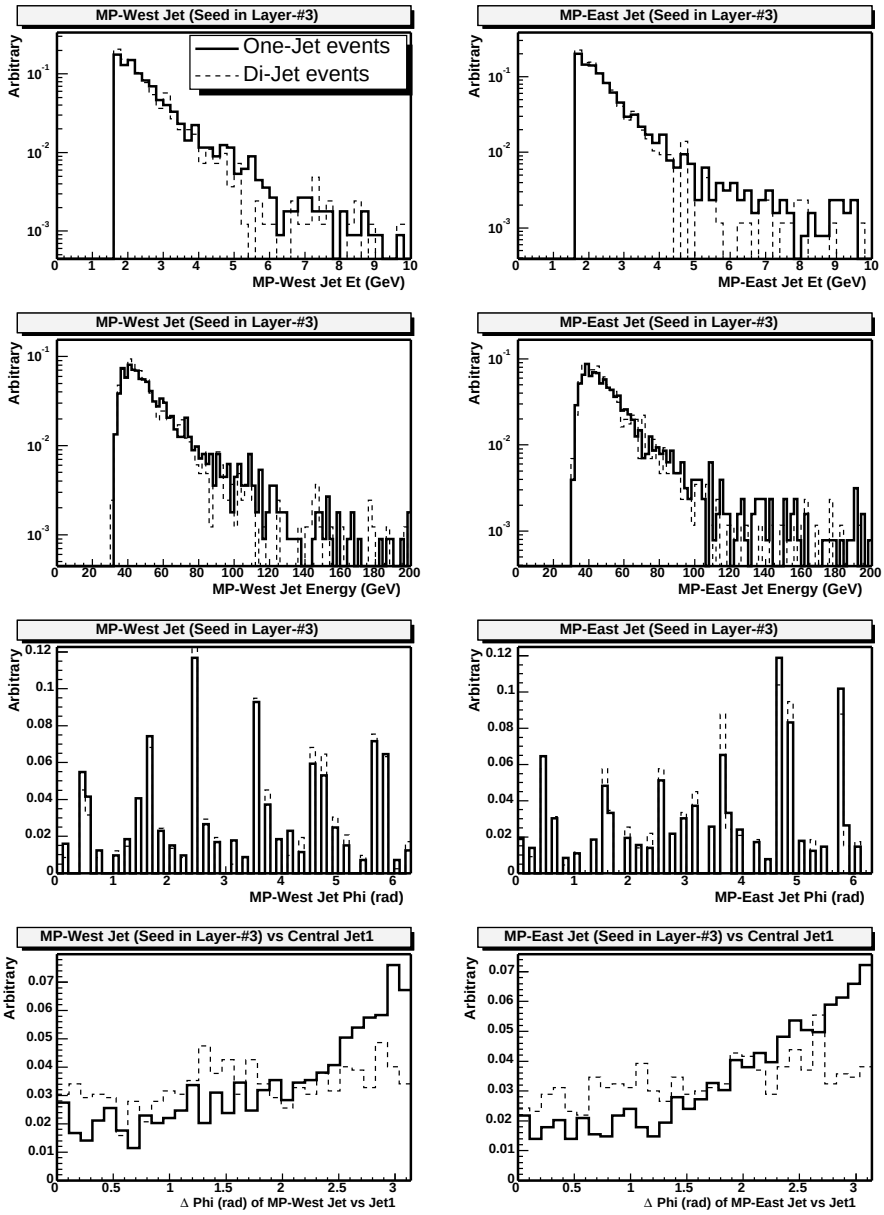

Figure 33: E_T (1st row), energy (2nd row), azimuthal angle ϕ (3rd row) and $\Delta\phi$ with respect to the leading jet in the central calorimeter (4th row) of the miniplug jets in one-jet (solid) and di-jet (dashed) samples of events with at most one miniplug jet in each detector.The distributions for the West (East) MiniPlug are shown in the left (right) side.

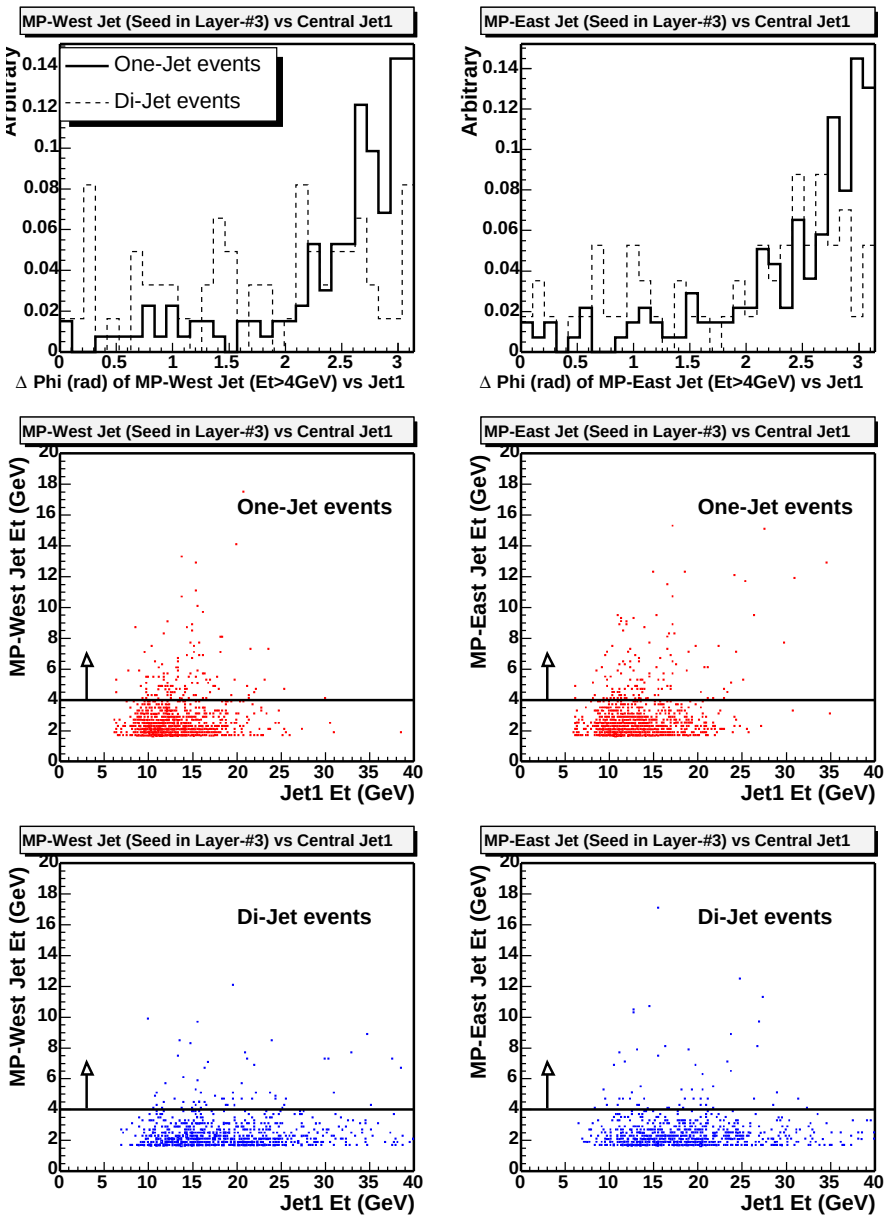

Figure 34: Top: $\Delta\phi$ of miniplug jet with respect to the leading jet in the Central calorimeter in one-jet (solid) and di-jet (dashed) samples. The E_T of miniplug jets are required to be greater than 4 GeV. Correlations between miniplug jet E_T and leading central jet E_T are shown in the middle for one-jet sample, and in the bottom for di-jet sample. The distributions for the West (East) MiniPlug are shown in the left (right) side.

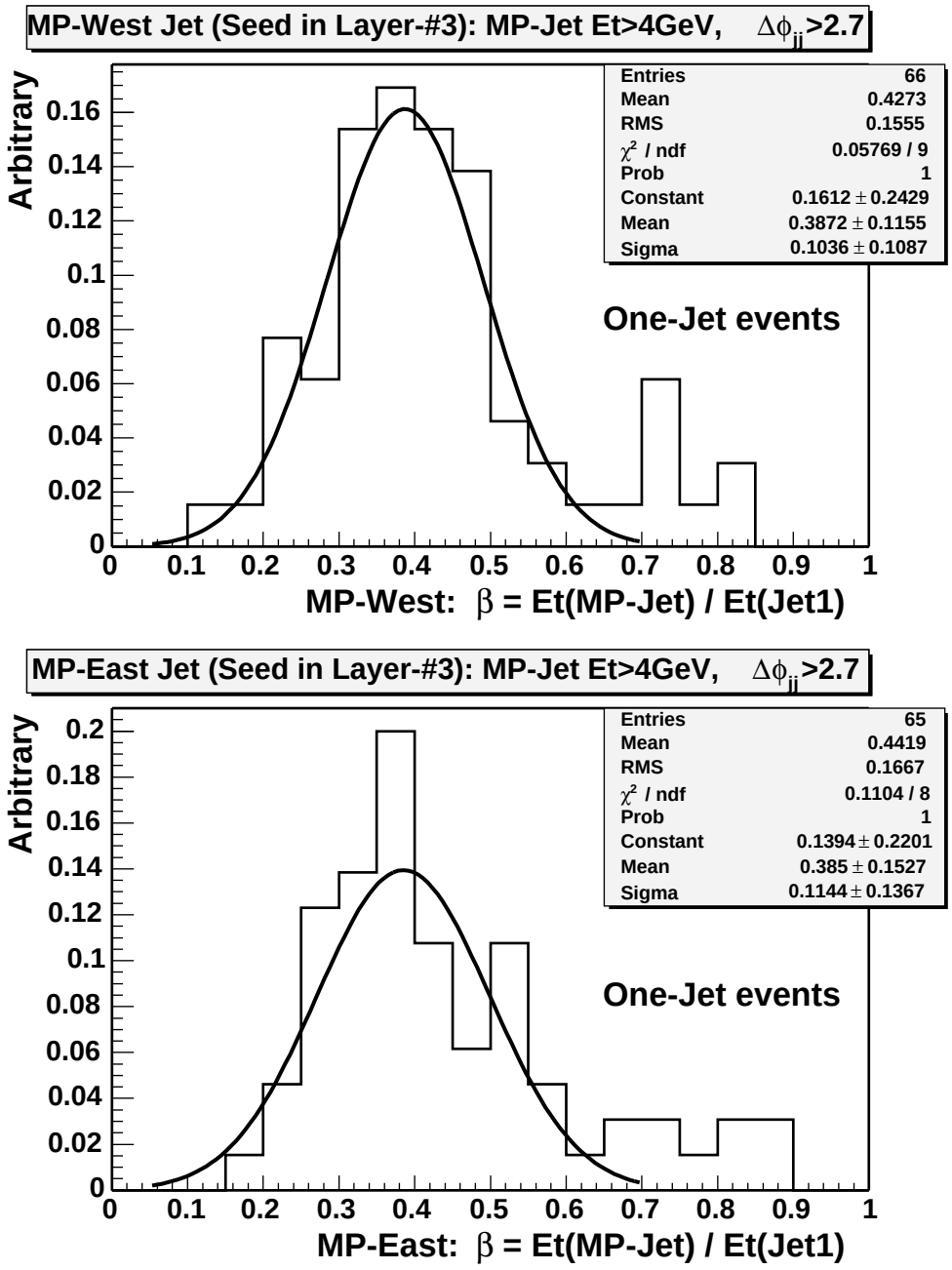

Figure 35: β (miniplug jet E_T divided by leading central jet E_T) distributions for events with a miniplug jet of $E_T > 4$ GeV and $\Delta\phi$ of miniplug-central jets greater than 2.7 in one-jet sample. Top (bottom) plot is for West (East) MiniPlug.

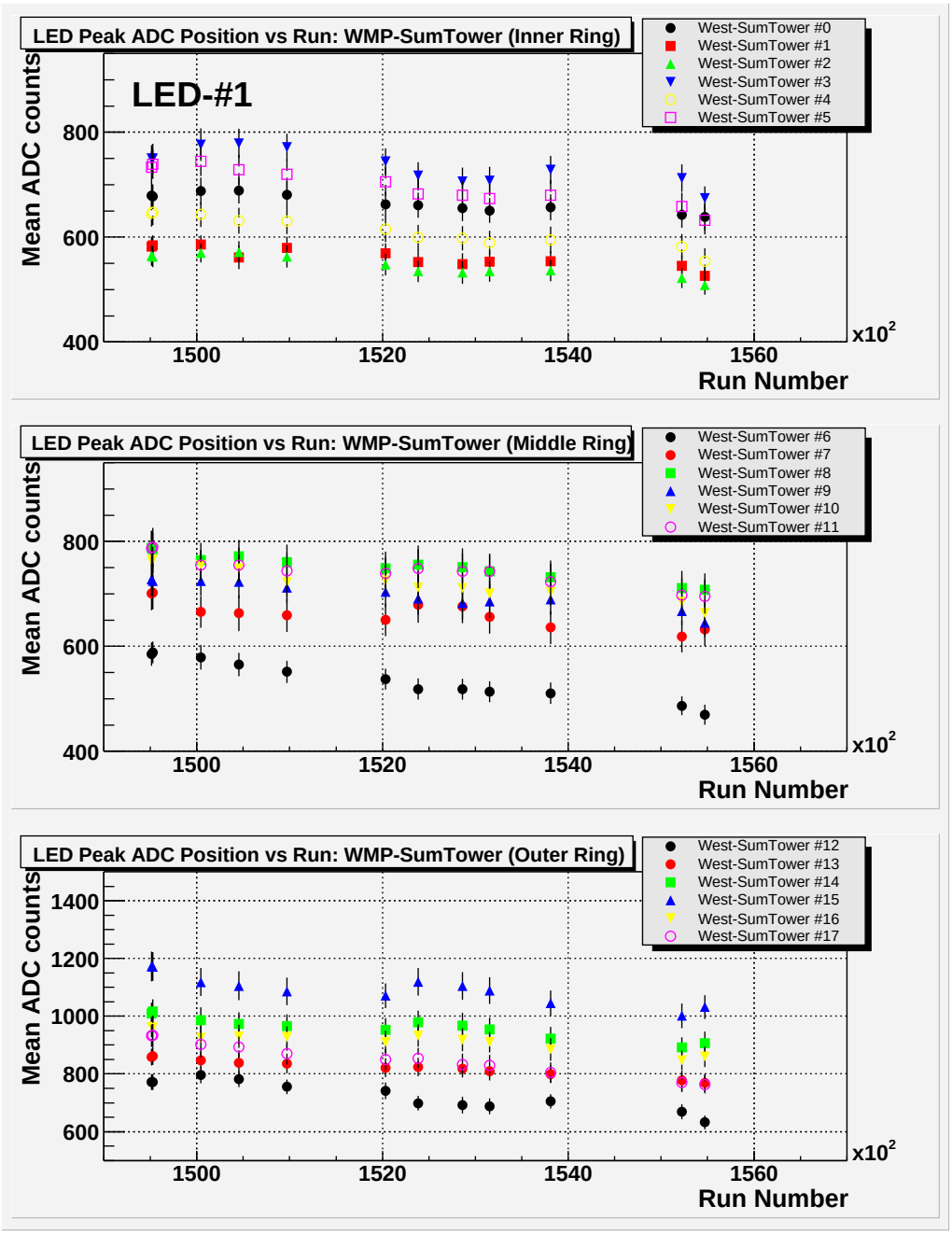

Figure 36: West MiniPlug detector response in LED calibration as a function of run number between Aug. 5th, 2002 and Dec. 18th, 2002. The inner, middle and outer ring PMTs are shown in the top, middle and bottom plots, respectively.

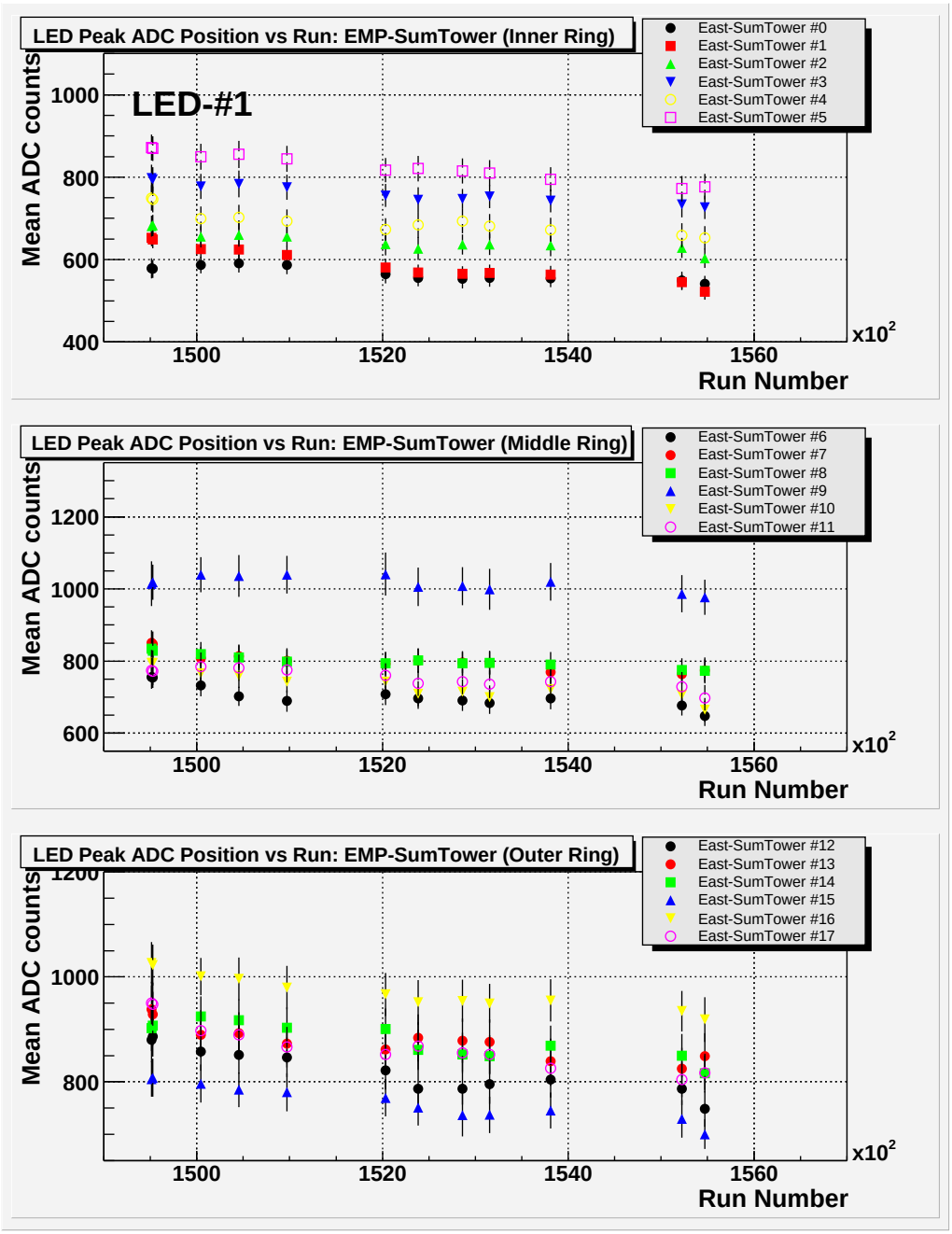

Figure 37: East MiniPlug detector response in LED calibration as a function of run number between Aug. 5th, 2002 and Dec. 18th, 2002. The inner, middle and outer ring PMTs are shown in the top, middle and bottom plots, respectively.